UNCLASSIFIED

SECURITY CLASSIFICATION OF THIS PAGE (When Data Entered)

REPORT DOCUMENTATION PAGE

READ INSTRUCTIONS BEFORE COMPLETING FORM

1. REPORT NUMBER

2. GOVT ACCESSION NO.

3. RECIPIENT'S CATALOG NUMBER

4. TITLE (and Subtitle)
An approximate technique for the integrations of the equations of motion in an FEL - ~~One dimensional Monte Carlo analysis of an FEL in a storage ring.~~

5. TYPE OF REPORT & PERIOD COVERED
Final Report, May [redacted] - June 77

6. PERFORMING ORG. REPORT NUMBER
HEPL 819 [redacted] HEPL-824

7. AUTHOR(s)
J. M. J./Madey, D. A. G./Deacon, L. R./Elias and T. I./Smith

8. CONTRACT OR GRANT NUMBER(s)
DASG-60-77-C-0083

9. PERFORMING ORGANIZATION NAME AND ADDRESS
Physics Department
Stanford University
Stanford, CA 94305

10. PROGRAM ELEMENT, PROJECT, TASK AREA & WORK UNIT NUMBERS
36p.

11. CONTROLLING OFFICE NAME AND ADDRESS
Ballistic Missile Defense Advanced Technology Center, ATTN: ATC-O, P. O. Box 1500
Huntsville, AL 35807

12. REPORT DATE
Sep[redacted] 1978

13. NUMBER OF PAGES
55

14. MONITORING AGENCY NAME & ADDRESS(if different from Controlling Office)

LEVEL II

15. SECURITY CLASS. (of this report)
UNCLASSIFIED

15a. DECLASSIFICATION/DOWNGRADING SCHEDULE

HEPL-819, HEPL-824

16. DISTRIBUTION STATEMENT (of this Report)

Approved for public release; distribution unlimited.

An Approximate Technique for the Integrations of the Equations of Motion in a Free Electron Laser (FEL). One Dimensional Monte Carlo Analysis of a Free Electron Laser (FEL) in a Storage Ring.

17. DISTRIBUTION STATEMENT (of the abstract entered in Block 20, if different from Report)

18. SUPPLEMENTARY NOTES

19. KEY WORDS (Continue on reverse side if necessary and identify by block number)
Free Electron Laser
Storage Ring
Equations of Motion
Calculational Techniques

20. ABSTRACT (Continue on reverse side if necessary and identify by block number)
The final report for this contract consists of two articles submitted for publication in the open literature. In the first article the authors describe an approximation they have used to compute gain, saturation, and electron statistics for a free electron laser. In the second article they report the results of a Monte Carlo method one-dimensional analysis of the equilibrium energy spread, bunch length, and average energy radiated by electrons in a storage ring free electron laser.

To be submitted
to Physical Review

HEPL 819
June 1978

(2)

AN APPROXIMATE TECHNIQUE FOR THE INTEGRATIONS OF THE EQUATIONS OF MOTION IN A FREE ELECTRON LASER*

J. M. J. Madey, D. A. G. Deacon,
L. R. Elias, and T. I. Smith

Physics Department and High Energy Physics Laboratory
Stanford University, Stanford, California 94305

*Supported in part by U.S. Army BMD-ATC under contract DASG-60-77-C-0083.

78 10 16 0

AN APPROXIMATE TECHNIQUE FOR THE INTEGRATIONS OF THE EQUATIONS OF MOTION IN A FREE ELECTRON LASER

J. M. J. Madey, D. A. D. Deacon,
L. R. Elias, and T. I. Smith

Physics Department and High Energy Physics Laboratory
Stanford University, Stanford, California 94305

ABSTRACT

We describe an approximation we have used to compute gain, saturation, and electron statistics at high power in the Stanford Free Electron Laser.

09 15 090

AN APPROXIMATE TECHNIQUE FOR THE INTEGRATIONS OF THE EQUATIONS OF MOTION IN A FREE ELECTRON LASER

1. Introduction

In the analysis of the free-electron laser (FEL) it is necessary to follow the motion of an electron beam as it moves through a long periodic magnetic field in the presence of an electromagnetic wave. We are interested in several aspects of the problem: 1) How much energy do the electrons transfer to the electromagnetic field? 2) What is the spread in the energy lost by the electrons? and 3) How do the gain and spread change when the amplitude of the wave is large?

When the optical power density is low, the phase and amplitude of the field cannot be defined with precision and it is necessary to employ a quantum formulation to analyze the evolution of the electron's trajectories.[1] When the optical power density is large or, alternatively, when the wave length is long, the classical approximation can be employed. The condition for the applicability of the classical approximation can be formulated as:

$$S_{lab} > \frac{1}{4\pi^{3/2}} \frac{\hbar\omega_0^3}{(1+\beta)\lambda_q c} \qquad (1)$$

where $S = (c/8\pi)(E \times H)$ is the optical power density, ω_0 is the optical frequency, λ_q the magnet period and $\hbar$ is Planck's constant.

Our interest in this paper lies in operation at high power, and we will assume the validity of the classical approximation. It is useful to consider two limiting cases. When the electron density is

large, the coulomb forces between electrons become comparable to the force due to the electric and magnetic fields and, since the gain can be large, the energy density of the electromagnetic field can change substantially during the interaction. In this limit, it is not practical to follow the motion of individual electrons and the problem is best pursued by treating the electron distribution as a charged fluid. Microwave power tubes such as klystrons, magnetrons and traveling wave tubes most commonly operate in this limit.

In the low-current limit the motion of electrons is unaffected by their neighbors, and so long as the gain is small the amplitude of the electromagnetic field changes only slightly during the interaction. In this case, it is possible to approximate the field as constant and to reduce the problem to the analysis of the motion of a single electron. The single particle approach is applicable when the Debye wavelength measured in the electron rest frame is large in comparison to the optical wavelength:

$$k_D^{-1} = \left(\frac{K\lambda}{4\pi n_0 e^2}\right)^{1/2} > \lambda \qquad (2)$$

and when the gain per pass is less than 3 dB. In contrast to the situation in microwave power tubes, the electron dnesity in the rest frame is typically small in devices involving the interaction of relativistic electrons at optical wavelengths. Devices such as the free-electron laser which operate at infrared and visible wavelengths can be described quite adequately by the single particle approximation.

A number of methods have been applied to analyze operations in

this limit. The first analysis was by Phillips who numerically integrated the Lorentz force equations in the single particle limit for a microwave power tube, the ubitron.[2] A number of authors have also developed numerical solutions to the collisionless Boltzmann equations[3,4] for the electron distribution in a FEL. The Boltzmann approach has the advantage of yielding a direct result for the distribution function, but the causal connection between the electrons' motion and the initial conditions is suppressed. Finally, Colson,[5] Bambini and Renieri[6], and Baier and Milstein[7] have derived an elegant transformation to relate the electrons' motion in a free-electron laser to the motion of a pendulum in a gravitational field. This transformation has been a powerful tool for the description of laser operation in both the small signal and saturation regimes.

The method described in this paper was first employed by Madey and Deacon.[8] This technique relates the solution of the Lorentz force equation in the presence of an optical field to the solutions of the force equation when only the dc magnetic field is present. The advantage of the technique is that it is directly applicable to the analysis of electron motion in periodic magnets of arbitrary geometry and it is well adapted for use in numerical calculations. Qualitatively, the method is interesting because the physical arguments justifying the approximation indicate that the laser interaction does not fundamentally alter the character of the electrons' trajectories in the periodic field. We will find that the principal effect of the optical field is simply to accelerate the electrons along trajectories which are locally indistinguishable from the trajectories they would follow when only the dc field is present.

78 10 16

2. Description of the Approximation

In a free-electron laser an electron beam is made to move through a spatially periodic transverse magnetic field. To be specific, we will assume that the electrons move along the $\hat{z}$ axis and that the magnetic field can be represented in the form:

$$\underset{\sim}{B}_o = \mathrm{Re}\,[\underset{\sim}{B}_o \exp i\,(\frac{2\pi}{\lambda_q})\,z] \tag{3}$$

where λ_q is the period of the field and the constant vector $\underset{\sim}{B}_o$ can be real or complex depending on the polarization. The transverse magnetic field causes the electrons' transverse position to oscillate with the period of the magnet. For a circularly polarized field the electrons will move in a helical trajectory, whereas a linear transverse field will result in planar motion.

The momentum $\underset{\sim}{p}_o$ and velocity $\underset{\sim}{\beta}_o c$ of an electron moving through the field in the absence of an optical field must satisfy the equation:

$$\frac{d\underset{\sim}{p}_o}{dt} = e\underset{\sim}{\beta}_o \times \underset{\sim}{B}_o \ . \tag{4}$$

This can be rewritten in the form:

$$\sqrt{\gamma^2-1}\;\frac{d\hat{\beta}_o}{dt} = (\frac{e}{mc})\,\underset{\sim}{\beta}_o \times \underset{\sim}{B}_o \tag{5}$$

where γmc^2 is the electron mass energy, $\hat{\beta}_o$ is the instantaneous direction of motion of the electrons ($|\hat{\beta}_o| \equiv 1$), and we have made use of the identities

$$\underset{\sim}{p}_o = \gamma \underset{\sim}{\beta}_o mc = \sqrt{\gamma^2 - 1}\ \hat{\beta}_o mc$$

$$\frac{d\gamma}{dt} = \frac{e}{mc}\ e\underset{\sim}{E} \cdot \underset{\sim}{\beta} \tag{6}$$

$= 0$ for a static magnetic field .

The objective is to determine the effect of the optical field on the trajectories. We will assume that the optical field can be represented as a plane wave:

$$\underset{\sim}{E} = \mathrm{Re}[\underset{\sim}{E}_o \exp i(\underset{\sim}{k} \cdot \underset{\sim}{r} - \omega t)$$

$$\underset{\sim}{B} = \hat{k} \times \underset{\sim}{E} \tag{7}$$

where $\underset{\sim}{K}$ is the propagation vector, $\omega = k/c$ and $\underset{\sim}{E}_o$ can be real or complex, depending on the polarization. In the presence of the optical field the electron momentum p and velocity β must satisfy the equation:

$$\frac{d\underset{\sim}{p}}{dt} = e[\underset{\sim}{E} + \underset{\sim}{\beta} \times \underset{\sim}{B}] + e\underset{\sim}{\beta} \times \underset{\sim}{B}_o \ . \tag{8}$$

We will show that the solution to equation (8) can be approximated by the solution to the modified equations:

$$\sqrt{\gamma^2 - 1}\ \frac{d\hat{\beta}}{dt} = \frac{e}{mc}\ \underset{\sim}{\beta} \times \underset{\sim}{B}_o \tag{9a}$$

$$\frac{d\gamma}{dt} = \frac{e}{mc}\ \underset{\sim}{\beta} \cdot \underset{\sim}{E} \ . \tag{9b}$$

The first equation relates the rate of change of $\hat{\beta}$ to $\underset{\sim}{\beta}$ and $\underset{\sim}{B}_o$. It is identical to the equation governing the motion of electrons in the static field when the optical field is absent. The radius of curvature of an electron with a given vector velocity in this approximation will therefore be identical to the curvature of an electron with the velocity when the optical field is absent. Equation (9b) relates the rate of change of energy to the dot product of the electron velocity and the electric field. Equation (9b) would be exact if $c\underset{\sim}{\beta}$ were the actual velocity.

With respect to the application of this approximation, we note that it is frequently possible to develop a general solution for the motion of an electron through a static periodic field in which $\underset{\sim}{\beta}$ is expressed as a function of the energy and position of the electron and the period, polarization, and amplitude of the static field. This means that the solution to equation (9a) will typically be available in either analytic or tabular form and only equation (9b) will need to be integrated, substantially reducing the effort required to integrate the equations of motion.

3. Estimation of Error

To estimate the error generated by the approximation we will develop a differential equation for the error term $\delta\underset{\sim}{p}$, the difference between the exact solution $\underset{\sim}{p}(t)$ and the approximation solution $\underset{\sim}{p}_a(t)$. If $\delta\underset{\sim}{p}$ is defined:

$$\delta\underset{\sim}{p}(t) \equiv \underset{\sim}{p}(t) - \underset{\sim}{p}_a(t) \ , \tag{10}$$

then $\delta\mathbf{p}$ satisfies the differential equation:

$$\frac{d\delta\mathbf{p}}{dt} = \frac{d\mathbf{p}(t)}{dt} - \frac{d\mathbf{p}_a(t)}{dt}$$

$$= e[\mathbf{E}(\mathbf{r},t) + \boldsymbol{\beta} \times \mathbf{B}(\mathbf{r},t)] \tag{11}$$

$$+ e\,\boldsymbol{\beta}\,\mathbf{B}_o(\mathbf{r}) - mc\left[\sqrt{\gamma_a^2-1}\;\frac{\partial\hat{\boldsymbol{\beta}}_a}{dt} - \frac{\hat{\boldsymbol{\beta}}_a\gamma_a}{\sqrt{\gamma_a^2-1}}\;\frac{d\gamma_a}{dt}\right]$$

where $\mathbf{r}$ is the exact electron position at the time t and $c\boldsymbol{\beta}$ is the exact velocity. We have defined $\gamma_a mc^2$ and $c\boldsymbol{\beta}_a$ as the approximate electron mass-energy and velocity, consistent with the designation of $\mathbf{p}_a$ as the approximate momentum, and have used equation (8) to express $d\mathbf{p}/dt$ in terms of the fields $\mathbf{E}$, $\mathbf{B}$, and $\mathbf{B}_o$.

If $\mathbf{r}$ and $\boldsymbol{\beta}$ were known, equation (11) could be integrated to obtain $\delta\mathbf{p}(t)$ using the values of γ_a and $\boldsymbol{\beta}_a$ computed from the approximation. Although we do not know $\mathbf{r}$ and $\boldsymbol{\beta}$, these quantities can be expressed in terms of $\mathbf{r}_a$ and $\boldsymbol{\beta}_a$, $\delta\mathbf{r}$ and $\delta\boldsymbol{\beta}$, where $\mathbf{r}_a$ is the approximate position of the electron and $\delta\mathbf{r}$ and $c\delta\boldsymbol{\beta}$ are the errors in position and velocity:

$$\mathbf{r}(t) = \mathbf{r}_a(t) + \delta\mathbf{r}(t)$$

$$\boldsymbol{\beta}(t) = \boldsymbol{\beta}_a(t) + \delta\boldsymbol{\beta}(t) \quad . \tag{12}$$

$\mathbf{r}_a$ and $\boldsymbol{\beta}_a$ can be defined in terms of $\mathbf{p}_a$ and γ_a:

$$\boldsymbol{\beta}_a = \frac{\mathbf{p}_a}{\gamma_a(t)mc}$$

$$\mathbf{r}_a = \mathbf{r}(t{=}0) + \int_0^t \boldsymbol{\beta}_a(t)dt \tag{13}$$

and $\delta\mathbf{r}$ and $\delta\boldsymbol{\beta}$ can similarly be expressed in terms of $\delta\mathbf{p}$:

$$\delta\boldsymbol{\beta} \approx \frac{\delta\mathbf{p}}{\gamma_a mc} - \left(\boldsymbol{\beta}_a \;\; \boldsymbol{\beta}_a \cdot \frac{\delta\mathbf{p}}{\gamma_a mc}\right)$$

$$\delta\mathbf{r} \approx \int_0^t c\delta\boldsymbol{\beta}\;\; dt \quad . \tag{14}$$

Under the assumption that $\delta\mathbf{r}$ is small in comparison to the magnet period and optical wavelength, the fields can be expanded as:

$$\mathbf{B}_o(\mathbf{r}) \approx (1 + \delta\mathbf{r}\cdot\nabla)\;\mathbf{B}_o(\mathbf{r}_a)$$

$$\mathbf{E}(\mathbf{r},t) \approx (1 + \delta\mathbf{r}\cdot\nabla)\;\;\mathbf{E}(\mathbf{r}_a,t) \tag{15}$$

$$\mathbf{B}(\mathbf{r},t) \approx (1 + \delta\mathbf{r}\cdot\nabla)\;\;\mathbf{B}(\mathbf{r}_a,t)$$

and equation (11) can be rewritten as:

$$\frac{d\delta\mathbf{p}}{dt} = e[\mathbf{E}(\mathbf{r}_a,t) + \boldsymbol{\beta}_a \times \mathbf{B}(\mathbf{r}_a,t)] + e\boldsymbol{\beta}_a \times \mathbf{B}_o(\mathbf{r}_a,t)$$

$$- (mc)[\sqrt{\gamma_a^2-1}\;\;\frac{\partial\hat{\boldsymbol{\beta}}_a}{\partial t} + \frac{\hat{\boldsymbol{\beta}}_a\gamma_a}{\sqrt{\gamma_a^2-1}}\;\;\frac{\partial\gamma_a}{\partial t}] + e[(\delta\mathbf{r}\cdot\nabla)\mathbf{E}(\mathbf{r}_a,t)$$

$$+ \delta\boldsymbol{\beta} \times \mathbf{B}_o(\mathbf{r}_a,t) + \boldsymbol{\beta}_o \times [(\delta\mathbf{r}\cdot\nabla)\mathbf{B}(\mathbf{r}_a,t)]$$

$$+ \delta\boldsymbol{\beta} \times \mathbf{B}(\mathbf{r}_a,t) + \boldsymbol{\beta}_o \times [(\delta\mathbf{r}\cdot\nabla)\mathbf{B}_o(\mathbf{r}_a)]] \quad . \tag{16}$$

Since $\delta\mathbf{r}$ and $\delta\boldsymbol{\beta}$ can be expressed in terms of $\delta\mathbf{p}$ and its integral, as shown in equation (14), equation (16) constitutes an integro-differential equation for $\delta\mathbf{p}$. Given the values $\mathbf{p}_a$, $\boldsymbol{\beta}_a$ and $\mathbf{r}_a$ from the approximation, equation (16) can be integrated to obtain the numerical value of each

of the error terms.

The driving terms in equation (16) are:

$$e[\underset{\sim}{E}(\underset{\sim}{r}_a,t) + \underset{\sim}{\beta}_a \times \underset{\sim}{B}(\underset{\sim}{r}_a,t)] + e\underset{\sim}{\beta}_a \times \underset{\sim}{B}_o(\underset{\sim}{r}_a,t)$$

$$-mc\left[\sqrt{\gamma_a^2-1}\ \frac{\partial\hat{\beta}_a}{\partial t} - \frac{\hat{\beta}_a\gamma_a}{\sqrt{\gamma_a^2-1}}\ \frac{\partial\gamma_a}{\partial t}\right]. \quad (17)$$

If this sum were equal to zero, equation (16) could be satisfied by setting $\delta\underset{\sim}{p} = \delta\underset{\sim}{\beta} = \delta\underset{\sim}{r} = 0$ and $\underset{\sim}{p}_a$ would be an exact solution. Although the individual terms in equation (17) will not be zero, we can show that the terms cancel to the order of $1/\gamma^2$. It is immediately seen from equation (9a) that $\left(\frac{e}{mc}\right)\underset{\sim}{\beta}_a \times \underset{\sim}{B}_o(\underset{\sim}{r}_a,t) - \sqrt{\gamma_a^2-1}\ \partial\hat{\beta}_a/\partial t = 0$. To demonstrate the cancellation of the remaining terms, we will define $\underset{\sim}{\beta}_\parallel \equiv \hat{z}(\beta_a\cdot\hat{z})$ and $\underset{\sim}{\beta}_\perp \equiv \underset{\sim}{\beta}_a - \underset{\sim}{\beta}_\parallel$ and note that the optical radiation in an FEL is usually assumed to propagate parallel to the z-axis ($\hat{n} = \hat{z}$). From equations (7) and (9b) it then follows that:

$$e[\underset{\sim}{E}(\underset{\sim}{r}_a,t) + \underset{\sim}{\beta}_a \times \underset{\sim}{B}(\underset{\sim}{r}_a,t)] - (mc)\,\frac{\hat{\beta}\gamma_a}{\sqrt{\gamma_a^2-1}}\ \frac{\partial\gamma_a}{\partial t}$$

$$= e[(1-\beta_\parallel)\underset{\sim}{E} + (1 - \frac{\beta_\parallel}{\beta_a^2})\ (\underset{\sim}{\beta}\cdot\underset{\sim}{E})\hat{z} - \frac{1}{\beta_a^2}\ (\underset{\sim}{\beta}\cdot\underset{\sim}{E})\underset{\sim}{\beta}_\perp]\ . \quad (18)$$

The magnitude of the terms on the right hand side of equation (18) is fixed by the magnitudes of $\underset{\sim}{\beta}_\parallel$ and $\underset{\sim}{\beta}_\perp$, the longitudinal and transverse velocities for an electron of the given energy moving through the static field $\underset{\sim}{B}_o$.

The canonical momentum of an electron moving through the

interaction region is $\underset{\sim}{p} + \frac{e\underset{\sim}{A}}{c}$ where A is the vector potential. Given the specifications of the magnetic field in equation (3) and the assumption $\hat{k} = \hat{z}$, the Lagrangian $(\underset{\sim}{p} + \frac{e\underset{\sim}{A}}{c})^2$ for an electron in the interaction region is independent of the transverse co-ordinates x and y. The transverse canonical momentum is, therefore, a constant of the motion. For typical operation conditions we can assume that the transverse canonical momentum $(\underset{\sim}{p} + \frac{e\underset{\sim}{A}}{c})_\perp = 0$. This follows from the requirement that the electron's average transverse kinetic momentum has to be minimized to limit the spread of the beam in the interaction region and to minimize the effect of transverse momentum on operating frequency and lineshape. If the transverse canonical momentum is zero, the transverse component of the kinetic momentum is $-\left(\frac{eA_\perp}{c}\right)$, and we have for the transverse component of $\underset{\sim}{\beta}$:

$$\underset{\sim}{\beta}_\perp - (\underset{\sim}{\beta}\cdot\hat{z})\hat{z} = \frac{\underset{\sim}{p} - (\underset{\sim}{p}\cdot\hat{z})\hat{z}}{\gamma mc} = -\frac{eA_\perp}{\gamma mc^2}\ . \quad (19)$$

Given eq. (6), the magnitude of $\beta_\perp$ and $\beta_\parallel$ is determined by the vector potential for the static field $\underset{\sim}{B}_o$. For a field with a period of λ_q and an amplitude $\underset{\sim}{B}_o$, the amplitude of the vector potential will be of the order of $(\lambda_q/2\pi)\underset{\sim}{B}_o$. For the circularly polarized magnetic field in the Stanford FEL:

$$|\beta_\perp| = \frac{e}{\gamma_a mc^2}\ \frac{\lambda_q B_o}{2\pi}$$

$$|\beta_\parallel| = \sqrt{\beta^2-\beta_\perp^2} \approx 1 - \frac{1}{2\gamma^2}\left[1 + \left(\frac{1}{2\pi}\right)^2\frac{\lambda_q^2 r_o B^2}{mc^2}\right] \quad (20)$$

for $\gamma \gg 1$.

If we assume these values for $\beta_\parallel$ and $\beta_\perp$, the individual terms in equation (18) have the form:

$$e(1-\beta_\parallel)\underline{E} \approx \frac{e}{2\gamma_a^2}\left[1+\left(\frac{\lambda_q eB_o}{2\pi mc^2}\right)^2\right]\underline{E}$$

$$\frac{e}{\beta_a^2}(\underline{E}\cdot\underline{\beta})\hat{\beta}_\perp \approx \frac{e}{\gamma_a^2}\left(\frac{\lambda_q eB_o}{2\pi mc^2}\right)^2 \frac{(\underline{E}\cdot\underline{\beta}_\perp)\underline{\beta}_\perp}{|\beta_\perp|^2} \tag{21}$$

$$e\left(1-\frac{\beta_\parallel}{\beta_a^2}\right)(\underline{E}\cdot\underline{\beta}_a)\hat{z} \approx -\frac{e}{2\gamma_a^2}\left(\frac{\lambda_q eB_o}{2\pi mc^2}\right)\left[1-\left(\frac{\lambda_q eB_o}{2\pi mc^2}\right)^2\right]\frac{(\underline{E}\cdot\underline{\beta}_\perp)}{|\beta_\perp|}\hat{z}\ .$$

The largest of these terms is of order eE/γ^2. We note that, although the numerical coefficients on the right hand side in equation (21) follow from the choice of circular polarization for the magnetic field, the cancellation of the terms to order $1/\gamma^2$ follows from the definition of the canonical momentum and is independent of polarization.

To estimate the magnitude of $\delta\underline{p}$ using equation (16) we will neglect the terms proportional to $\delta\underline{r}$ and $\delta\underline{\beta}$ and apply the triangle and Cauchey-Schwartz inequalities to generate an upper bound for $|\delta\underline{p}|$. The neglect of the terms containing $\delta\underline{r}$ and $\delta\underline{\beta}$ is justified by the observation that $\delta\underline{r}$ and $\delta\underline{\beta}$ are of order $\delta\underline{p}/\gamma$ or $\delta\underline{p}/\gamma^3$ and that the terms containing $\delta\underline{r}$ and $\delta\underline{\beta}$ are linear in the field amplitudes E, and B_o. The fractional error introduced in $\delta\underline{p}$ by the neglect of $\delta\underline{r}$ and $\delta\underline{\beta}$ in equation (16) will therefore be at most of order E/γ or B_o/γ and will approach zero in the relativistic limit.

If equation (21) is used to reduce the driving terms in equation (16) and the terms proportional to $\delta\underline{r}$ and $\delta\underline{\beta}$ are dropped, we obtain:

$$\frac{d\delta\underline{p}}{dt} \approx \frac{e}{\gamma_a^2}\Big\{\frac{1}{2}\left[1+\left(\frac{\lambda_q eB_o}{2\pi mc^2}\right)^2\right]\underline{E} + \left(\frac{\lambda_q eB_o}{2\pi mc^2}\right)^2\frac{(\underline{E}\cdot\underline{\beta}_\perp)\underline{\beta}_\perp}{|\beta_\perp|^2}$$
$$-\frac{1}{2\gamma_a}\left(\frac{\lambda_q eB_o}{2\pi mc^2}\right)\left[1-\left(\frac{\lambda_q eB_o}{2\pi mc^2}\right)^2\right]\frac{(\underline{E}\cdot\underline{\beta}_\perp)\hat{z}}{|\beta_\perp|}\Big\}\ . \tag{22}$$

If we define $\delta\underline{p}_\parallel \equiv (\delta\underline{p}\cdot\hat{z})\hat{z}$ and $\delta\underline{p}_\perp \equiv \delta\underline{p} - \delta\underline{p}_\parallel$, equation (22) can be further reduced to the equations:

$$\frac{d}{dt}\delta\underline{p}_\parallel = -\frac{e}{2\gamma_a^3}\left(\frac{\lambda_q eB_o}{2\pi mc^2}\right)\left[1-\left(\frac{\lambda_q eB_o}{2\pi mc^2}\right)^2\right]\frac{(\underline{E}\cdot\underline{\beta}_\perp)}{|\beta_\perp|}\hat{z} \tag{23a}$$

$$\frac{d}{dt}\delta\underline{p}_\perp = \frac{e}{\gamma_a^2}\Big\{\frac{1}{2}\left[1+\left(\frac{\lambda_q eB_o}{2\pi mc^2}\right)^2\right]\underline{E} + \left(\frac{\lambda_q eB_o}{2\pi mc^2}\right)^2\frac{(\underline{E}\cdot\underline{\beta}_\perp)}{|\beta_\perp|^2}\times\underline{\beta}_\perp\Big\}\ . \tag{23b}$$

Applying the triangle and Cauchey-Schwartz inequalities we have:

$$|\delta\underline{p}_\parallel(T)| < \frac{e}{2\gamma_a^3}\left(\frac{\lambda_q eB_o}{2\pi mc^2}\right)\left|1-\left(\frac{\lambda_q eB_o}{2\pi mc^2}\right)^2\right|\int_0^T dt\,\frac{|\underline{E}\cdot\underline{\beta}_\perp|}{|\beta_\perp|}$$
$$< \frac{e}{2\gamma_a^3}\left(\frac{\lambda_q eB_o}{2\pi mc^2}\right)\left|1-\left(\frac{\lambda_q eB_o}{2\pi mc^2}\right)^2\right|\,|E|T \tag{24}$$

$$|\delta\underline{p}_\perp(T)| < \frac{e}{\gamma_a^2}\int_0^T dt\,\Big\{\frac{1}{2}\left[1+\left(\frac{\lambda_q eB_o}{2\pi mc^2}\right)^2\right]|\underline{E}| + \left(\frac{\lambda_q eB_o}{2\pi mc^2}\right)^2\frac{|\underline{E}\cdot\underline{\beta}_\perp|}{|\beta_\perp|}\Big\}$$
$$< \frac{e}{\gamma_a^2}\Big\{\frac{1}{2}\left[1+\left(\frac{\lambda_q eB_o}{2\pi mc^2}\right)^2\right] + \left(\frac{\lambda_q eB_o}{2\pi mc^2}\right)^2\Big\}\,|E|\,T$$

where the interaction is assumed to start at $t = 0$ and to end at $t = T$, and $|E|$ and $|\beta_\perp|$ are understood to be the maximum values of the field and transverse velocity in the interaction region.

The actual magnitudes of $\delta\underline{p}_\parallel$ and $\delta\underline{p}_\perp$ will be influenced by the time dependence of the right hand side of equation (23). If the right

hand side is nearly constant in time as in the case of $\frac{d}{dt}\,\delta p_{\parallel}$ [Eq. (23a)], $\delta p_{\parallel}$ can approach the magnitude of the upper bound derived in equation (24). But if the right hand side oscillates rapidly during the interaction as in the case of $\frac{d}{dt}\,\delta p_{\perp}$ [Eq. (23b)], the upper bound in equation (24) will be a conservative estimate of the magnitude. The right hand side of equation (23b) oscillates with the magnet period and in this case a better estimate of the magnitude of $\delta p_{\perp}$ could plausibly be attained by setting T equal to the time required to traverse one magnet period.

Given the upper bounds from $\delta p_{\parallel}$ and $\delta p_{\perp}$ from equation (24), we can easily derive upper bounds for the error in energy δE and for the position error $\delta \underline{r}$. From $E^2 = (\underline{p}_a + \delta \underline{p})^2 c^2 + m^2 c^4$ we have:

$$\frac{\delta E}{E} = \frac{2\underline{p}_a \cdot \delta \underline{p}}{p^2 + m^2 c^2} \ . \tag{25}$$

While from equation (14) we have:

$$\begin{aligned} |\delta \underline{r}_{\parallel}| &< cT\,|\delta \underline{\beta}_{\parallel}| \approx cT\,\frac{|\delta p_{\parallel}|}{\gamma_a^3 mc} \\ |\delta \underline{r}_{\perp}| &< cT\,|\delta \underline{\beta}_{\perp}| \approx cT\cdot\frac{|\delta p_{\perp}|}{\gamma_a mc} \end{aligned} \tag{26}$$

where $\delta\underline{\beta}_{\parallel}$, $\delta\underline{\beta}_{\perp}$, $\delta \underline{r}_{\parallel}$ and $\delta \underline{r}_{\perp}$ have been defined consistent with the previous definitions of $\delta p_{\parallel}$ and $\delta p_{\perp}$ as the projections on the z-axis and on the plane normal z. We note that the relationship utilized in equation (26) between the longitudinal components of $\delta \underline{p}$ and $\delta \underline{\beta}$ and the transverse components of these vectors differ because the

increment of velocity is in one case parallel to the direction of motion and in the other case it is assumed to be normal to $\underline{p}$.

For the Stanford Free-Electron Laser, which operated with a 43 MeV electron beam at a wavelength of 3 microns, the magnet period was 3.2 cm, and the interaction length was 5.2 meters. The power density in the interaction region at saturation was approximately 10^7 watts/cm^2. Using equation (20) to compute $\beta_{\parallel}$ and $\beta_{\perp}$ for the helical magnet and equation (24) to compute the upper bounds to $\delta p_{\parallel}$ and $\delta p_{\perp}$, we obtain for $\delta \underline{p}$, δE and $\delta \underline{r}$ at saturation:

$$\begin{aligned} &\frac{\delta p_{\parallel}}{p} < 1.5 \times 10^{-6} \\ &\frac{\delta p_{\perp}}{p} < 8.8 \times 10^{-4} \\ &\frac{\delta E}{E} < 3.2 \times 10^{-6} \\ &|\delta r_{\parallel}| < 1.2 \times 10^{-7}\ \text{cm} \\ &|\delta r_{\perp}| < 0.45\ \text{cm}\ . \end{aligned} \tag{27}$$

We note that the error in $\delta r_{\parallel}$ is less than 12 Å, consistent with the assumption that $\delta r_{\parallel}$ is small in comparison to the optical wavelength. The fractional error $\delta E/E$ in energy is less than 3.2×10^{-6}. By comparison, the average fractional energy loss and RMS spread in energy for these operating conditions are of the order of 1×10^{-2} (see Figures 2 and 3). It is apparent that the errors in the axial

position and momentum computed using this approximation are very small.

The limits on $\delta r_\perp$ and $\delta p_\perp$ are not so impressive. In part, the problem arises from the oscillatory nature of the integrand in equation (23b). The integrand reverses sign every magnet period whereas, in the upper bound developed using the triangle inequality in equation (24), the integrand is taken to be positive definite. Unfortunately, the only reliable means to estimate the size of $\delta p_\perp$ and $\delta r_\perp$ in comparison to the upper bounds in equation (27) would be to integrate equations (14b) and (23b), a technique which can be applied only on a case-by-case basis.

We can conclude that, in situations comparable to this example, the approximation is entirely adequate for the analysis of the energy radiated by the electrons during their passage through the periodic field. We cannot be so confident of the approximation's representation of the effect of the interaction on the transverse momentum of the electrons. The use of the approximation in cases in which the transverse momentum is of interest will have to be justified by the explicit integration of the equations for $\delta\dot{p}_\perp$ and $\delta\dot{r}_\perp$.

4. Application to the Analysis of FEL Operation

As an example of an application of this technique, we can analyze the operation of the Stanford Free-Electron Laser in the single pass configuration and examine the effect of variation of the magnet period on the gain and electron momentum spectrum. If the

circularly polarized magnetic field is expressed in the form:

$$\underline{B}_o = B_o\,[\hat{x}\cos\left(\frac{2\pi z}{\lambda_q}\right) + \hat{y}\sin\left(\frac{2\pi z}{\lambda_q}\right)] \quad (28)$$

and we restrict consideration to trajectories in which the transverse canonical momentum is zero, the solution to equation (a) has the form:

$$\underline{\beta}(t) = \{1 - \frac{1}{\gamma^2}[1 + \left(\frac{1}{2\pi}\right)^2\left(\frac{\lambda_q^{\,2} r_o B^2}{mc^2}\right)]\}^{1/2}\hat{z} + \left(\frac{\lambda_q e B_o}{2\pi\gamma mc^2}\right)\left(\hat{x}\cos\left(\frac{2\pi z}{\lambda_q}\right) + \hat{y}\sin\left(\frac{2\pi z}{\lambda_q}\right)\right)$$

$$\beta_\parallel \simeq \{1 - \frac{1}{2\gamma_s^{\,2}}[1 + \left(\frac{1}{2\pi}\right)^2\left(\frac{\lambda_q^{\,2} r_o B^2}{mc^2}\right)]\}c \quad (29)$$

$$\beta_\perp = \lambda_q e B_o / 2\pi\gamma_s mc^2 \ .$$

We note that the magnitude of $\beta_\parallel$ and $\beta_\perp$ depend only on λ_q, B_o and γ_s and are independent of position. From equation (9b):

$$\frac{d\gamma_s}{dt} = \frac{e}{mc}\,\underline{\beta}\cdot\underline{E} = \frac{e}{mc}\,|\underline{\beta}_\perp|\,|\underline{E}|\cos\theta \quad (30)$$

where θ is the phase angle between the transverse momentum and the electric field:

$$\theta = (\omega t - kz) - \frac{2\pi z}{\lambda_q} \ . \quad (31)$$

To integrate equation (30), we need to know the dependence of θ on time. The time derivative of θ can be expressed as:

$$\frac{d\theta}{dt} = \omega - (k + \frac{2\pi}{\lambda_q}) \beta_\parallel c$$

$$= \omega - c(k + \frac{2\pi}{\lambda_q}) \{1 - \frac{1}{\gamma_a^2} [1 + \left(\frac{1}{2\pi}\right)^2 \frac{\lambda_q^2 r_o B^2}{mc^2}]\}^{1/2} \quad . \tag{32}$$

The time derivatives of γ_a and θ can be converted to derivatives in z by division by $\beta_\parallel c$, leading to the coupled equations:

$$\frac{d\gamma}{dz} = \frac{e}{mc^2} \frac{|\beta_\perp|}{|\beta_\parallel|} |E| \cos\theta$$

$$\frac{d\theta}{dz} = \frac{1}{\beta_\parallel c} [\omega - \beta_\parallel c \; (k + \frac{2\pi}{\lambda_q})] \tag{33}$$

in which $\beta_\parallel$ and $\beta_\perp$ vary with γ_a according to equation (29). This system of equations can be integrated by elementary numerical methods.

If the electron energy is close to the "resonance energy" $\gamma_r mc^2$ defined by:

$$\omega = c(k + \frac{2\pi}{\lambda_q}) \{1 + \frac{1}{\gamma_r^2} [1 + \left(\frac{1}{2\pi}\right)^2 \left(\frac{\lambda_q r_o B^2}{mc^2}\right)]\}^{1/2} \tag{34}$$

and $\gamma_r \gg 1$, the derivative $d\theta/dt$ can be approximated by:

$$\frac{d\theta}{dt} \approx c(k + \frac{2\pi}{\lambda_q}) [1 + \left(\frac{1}{2\pi}\right)^2 \left(\frac{\lambda_q^2 r_o B^2}{mc^2}\right)] \frac{(\gamma - \gamma_r)}{\gamma_r^3} \tag{35}$$

Equation (35) can be used to express $d\gamma_r/dt$ in terms of $d^2\theta/dt^2$. We note that Colson's pendulum equation[4] can be obtained by combining this result with Eq. (30).

We note also that it is possible to use equation (9) to analyze the effects of variations in the magnitude of B_o and the period of

the static field. If the field strength and period vary with z, the vector potential will have the form:

$$\underset{\sim}{A}(z) = \frac{\lambda_q(z)}{2\pi} \quad B_o(z) \left[\hat{y}\cos\left(\frac{2\pi z}{\lambda_q(z)}\right) + \hat{x}\sin\left(\frac{2\pi z}{\lambda_q(z)}\right)\right] . \tag{36}$$

If $\underset{\sim}{A}$ is assumed to be independent of x and y, the transverse component of the canonical momentum remains a constant of the motion and the velocity $\underset{\sim}{\beta}c$ can be computed using equation (29) setting $B = B_o(z)$ and $\lambda_q = \lambda_q(z)$. The magnet period must also be made a function of position in equations (32) and (35) for $d\theta/dt$ and $d\theta/dz$. With these modifications, equations (33) can be integrated directly to compute the approximate electron energy and phase as functions of z.

While the initial value of γ_a is fixed by the energy with which the electrons enter the interaction region, the initial value of θ is not determined for a continuous electron beam. The change in the value of γ_o at the end of the interaction region as θ $(t = 0)$ varies between 0 and 2π leads to a spread in energy of the electrons emerging from the laser. The mean electron energy loss and the RMS energy spread can be computed by means of the appropriate averages over the inital phase.

The data in Figures 1-4 illustrate the application of the approximation. The data in Figure 1 shows a histogram for the final electron energy at an optical power density of 10^7 watts/cm^2 for the constant period helix used in the Stanford FEL. The initial phase was varied in steps of $\pi/100$ between 0 and 2π. Figure 2 shows the dependence of the maximum available gain on optical power density

for the Stanford magnet. Note that the available gain falls off at 1/5 at high power. Figures 3 and 4 show the dependence of gain and the spread on electron energy for two different magnet geometries. The data in Figure 3 shows a simple constant period helix. In Figure 4 the spread has been reduced and the gain increased by systematically increasing the magnet period starting with 3.20 centimeters and ending with 3.22 centimeters at the end of the interaction region.

We thank Dr. W. B. Colson for his comments concerning this problem.

FIGURE CAPTIONS

Figure 1: The figure shows a histogram for the final electron energy for the Stanford Free-Electron Laser computed using the approximation described in the text. The horizontal axis indicates the final electron energy. The vertical axis indicates the number of electrons falling into each energy bin as the inital phase was varied between zero and 2π in steps of $\pi/50$ radians. The magnet period was 3.2 cm, the magnet length 5.2 meters, and the magnetic field strength 2.3 kilogauss. The optical wavelength was 3μ and the optical power density 10^7 watts/cm^2. The initial electron energy was 42.19 MeV and was chosen to maximize the gain available at this power density.

Figure 2: The figure shows the dependence of the fractional gain per pass on the optical power density for the magnet used in the Stanford FEL. The data is for an optical wavelength of 3μ.

Figure 3: The figure shows the dependence on electron energy of relative optical gain and the RMS spread in electron energy for the magnet in the Stanford FEL. The data is for an optical wavelength of 3μ and an optical power density of 10^7 watts/cm^2.

Figure 4: The figures shows the dependence on electron energy of the relative optical gain and the RMS spread in electron energy. The data is for a 160 period magnet in which the period was increased linearly from 3.20 cm at the start of the interaction region to 3.22 cm at the end. The optical wavelength and power density are the same as in Figure 3.

REFERENCES

1. J. M. J. Madey and D. A. G. Deacon, in Cooperative Effects in Matter and Radiation, C. M. Bowden, D. W. Howgate and H. H. Robl, eds. (Plenum Press, 1977) p. 313.
2. R. M. Phillips, IRE Transactions on Electron Devices 1 (1960) p. 231.
3. F. A. Hopf, P. Meystre, M. O. Scully, and W. H. Louisell, Opt. Comm. 18 (1976) 413.

   F. A. Hopf, P. Meystre, M. O. Scully, and W. H. Louisell, Phys. Rev. Lett. 37 (1976) 1342.

   H. Al-Abawi, F. A. Hopf, and P. Meystre, Phys. Rev. A 16 (1977)
4. W. B. Colson, Phys. Lett. 64A (1977) 190.
5. A. Bambini and A. Renieri, The Free Electron Laser: A Single Particle Classical Model, Nuovo Cimento 21 (1978) 399.
6. V. N. Baier and A. I. Milstein, Phys. Lett. 65A (1978) 319.

SYMBOLS

Physical Constants

- e = electron charge (4.8×10^{-10} statcoulombs)
- m = electron mass (9.11×10^{-28} grams)
- c = speed of light (3×10^{10} cm sec^{-1})
- $\hbar$ = Planck's constant (1.05×10^{-27} erg-sec)
- K = Boltzmann's constant (1.38×10^{-16} erg °K^{-1})

Electron Coordinates

- $\mathbf{r}$ = exact electron position
- $\mathbf{r}_a$ = approximate electron position calculated using approximation described in text for analysis of electron motion in presence of optical field.
- $\delta\mathbf{r}$ = $\mathbf{r} - \mathbf{r}_a$ = position error
- $\delta\mathbf{r}_{\parallel}$ = $(\delta\mathbf{r}\cdot\hat{z})\hat{z}$ = longitudinal position error
- $\delta\mathbf{r}_{\perp}$ = $\delta\mathbf{r}-\delta\mathbf{r}_{\parallel}$ = transverse position error
- $\boldsymbol{\beta}$ = $\dot{\mathbf{r}}/c$ = exact normalized electron velocity
- $\boldsymbol{\beta}_o$ = normalized electron velocity when optical field is absent
- $\hat{\beta}_o$ = $\boldsymbol{\beta}_o/|\boldsymbol{\beta}_o|$ = unit vector for normalized velocity when optical field is absent
- $\boldsymbol{\beta}_a$ = approximate normalized velocity, calculated using approximation described in text to analyze electron motion in presence of optical field.
- $\boldsymbol{\beta}_{\parallel}$ = $(\boldsymbol{\beta}_a\cdot\hat{z})\hat{z}$ = normalized approximate longitudinal velocity
- $\boldsymbol{\beta}_{\perp}$ = $\boldsymbol{\beta}_a - \boldsymbol{\beta}_{\parallel}$ = normalized approximate transverse velocity
- $\delta\boldsymbol{\beta}$ = $\boldsymbol{\beta} - \boldsymbol{\beta}_a$ = normalized velocity error
- $\delta\boldsymbol{\beta}_{\parallel}$ = $(\delta\boldsymbol{\beta}\cdot\hat{z})\hat{z}$ = normalized longitudinal velocity error
- $\delta\boldsymbol{\beta}_{\perp}$ = $\delta\boldsymbol{\beta} - \delta\boldsymbol{\beta}_{\parallel}$ = normalized transverse velocity error

$\underset{\sim}{p}$ = exact electron momentum (gm-cm-sec^{-1})

$\underset{\sim}{p}_o$ = electron momentum when optical field is absent

$\underset{\sim}{p}_a$ = approximate electron momentum calculated using approximation described in text for analysis of electron motion in presence of optical field.

$\delta\underset{\sim}{p}$ = $\underset{\sim}{p} - \underset{\sim}{p}_a$ = momentum error

$\delta\underset{\sim}{p}_{\parallel}$ = $(\delta\underset{\sim}{p}\cdot\hat{z})\hat{z}$ = longitudinal momentum error

$\delta\underset{\sim}{p}_{\perp}$ = $\delta\underset{\sim}{p} - \delta\underset{\sim}{p}_{\parallel}$ = transverse momentum error

γ = $\sqrt{p^2+m^2c^2}/mc$ = exact normalized electron mass-energy

γ_a = approximate electron mass-energy, calculated using approximation described in text for analysis of electron motion in presence of optical field.

$\delta\gamma$ = $\gamma - \gamma_a$ = error in normalized energy

Optical Field Coordinates

ω = optical frequency (sec^{-1})

$\underset{\sim}{k}$ = optical wave vector (cm^{-1})

$\hat{k}$ = $\underset{\sim}{k}/|k|$ = unit wave vector

$\underset{\sim}{E}$ = optical electric field (stat colts cm^{-1})

$\underset{\sim}{B}$ = optical magnetic field (gauss)

$\underset{\sim}{\varepsilon}_o$ = polarization vector for optical electric field

S_{lab} = optical power density (ergs cm^{-2} sec^{-1})

Magnet Geometry

λ_q = magnet period (cm)

L = length (cm)

B_o = static magnetic field (gauss)

$\underset{\sim}{B}_o$ = polarization vector for static magnetic field.

$\underset{\sim}{A}$ = vector potential for static magnetic field

$\underset{\sim}{A}_{\perp}$ = $\underset{\sim}{A} - (\underset{\sim}{A}\cdot\hat{z})\hat{z}$ = transverse component of vector potential

Miscellaneous

t = dummy variable for time

T = total interaction time (sec)

K_D = debye wave number

n_o = electron density (cm^{-3})

τ = temperature (°K)

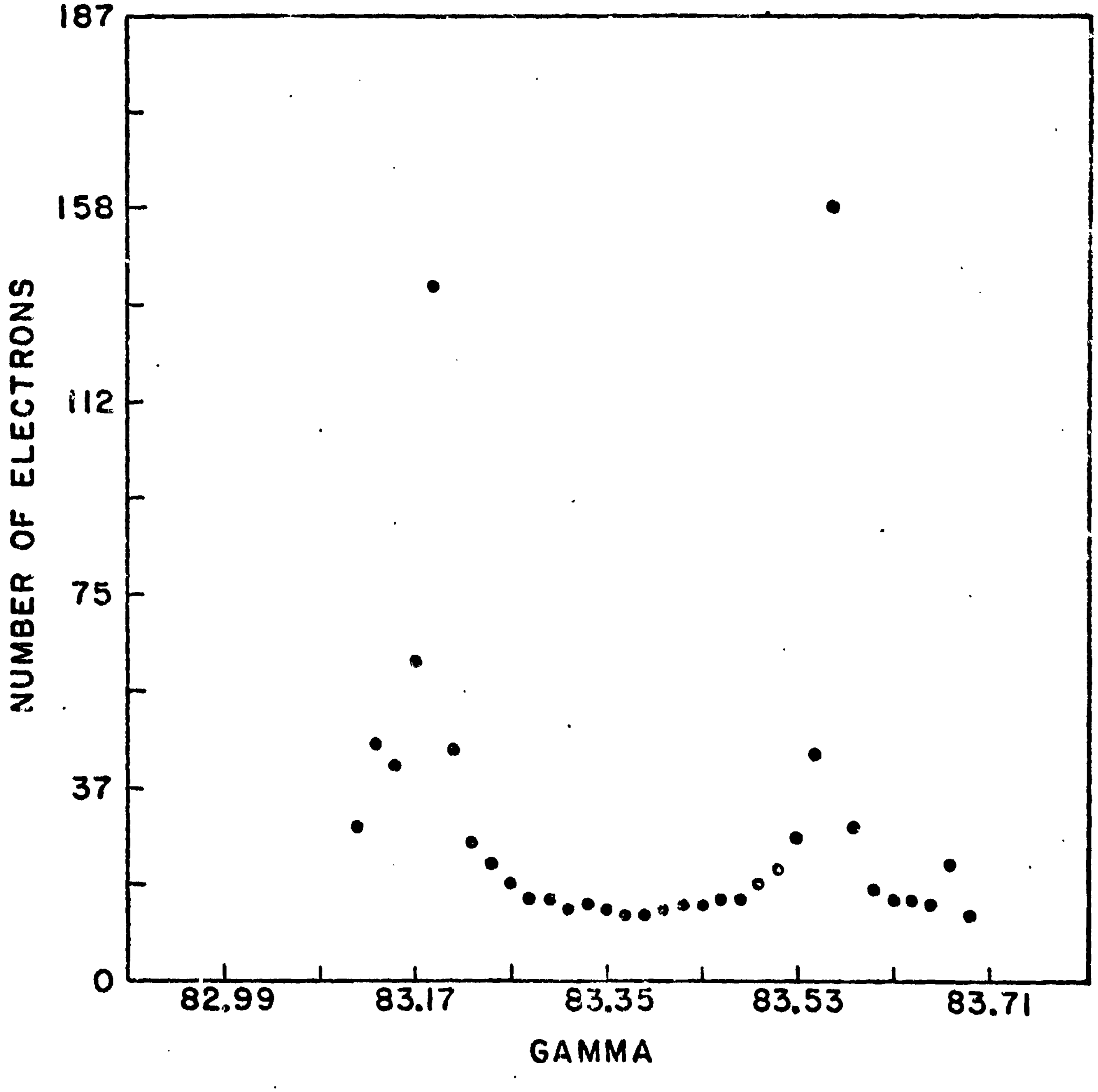

NUMBER OF ELECTRONS
187
158
112
75
37
0
82.99
83.17
83.35
83.53
83.71
GAMMA

Figure 1

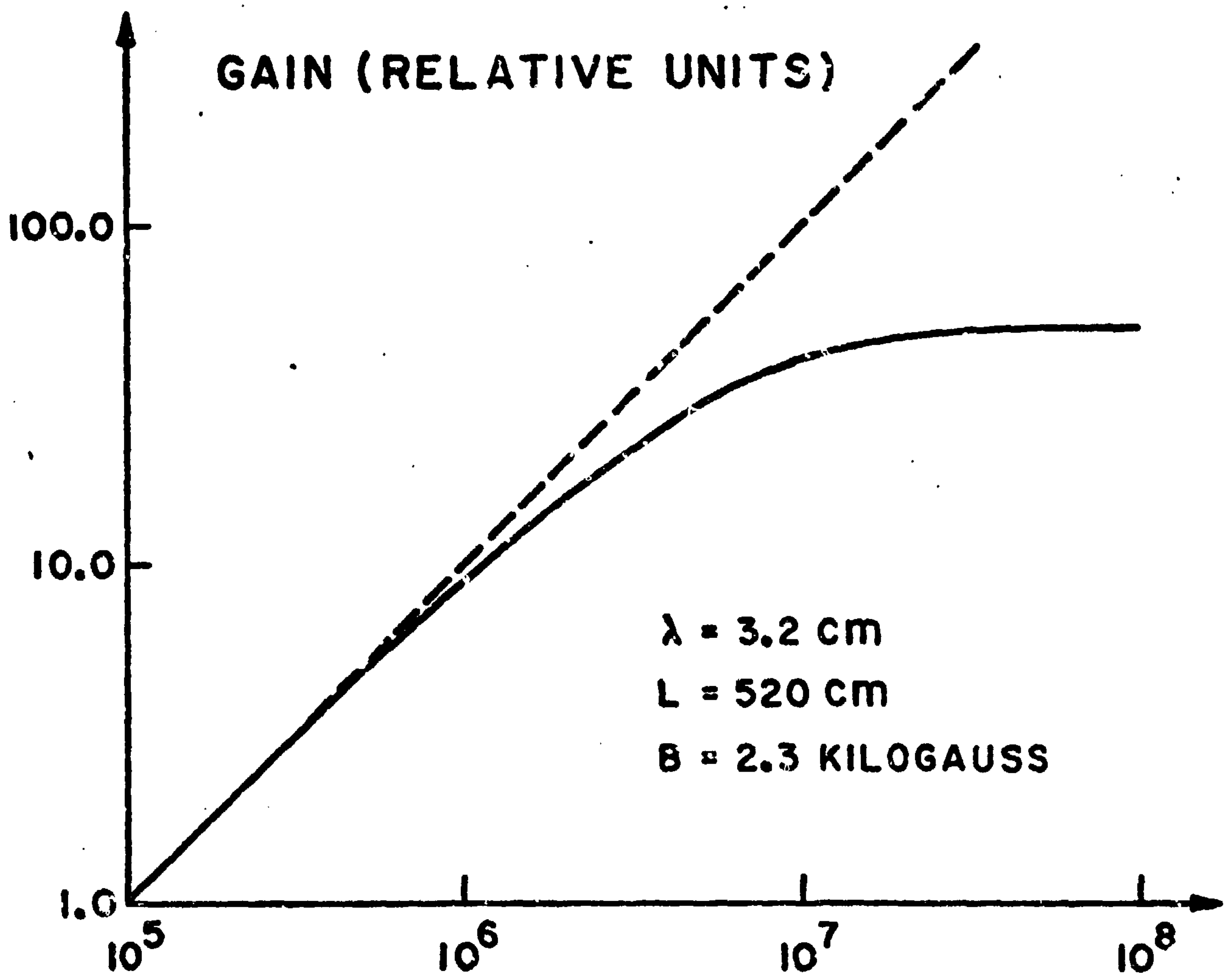
GAIN (RELATIVE UNITS)
100.0
10.0
1.0
λ = 3.2 cm
L = 520 cm
B = 2.3 KILOGAUSS
10^5
10^6
10^7
10^8

Figure 2

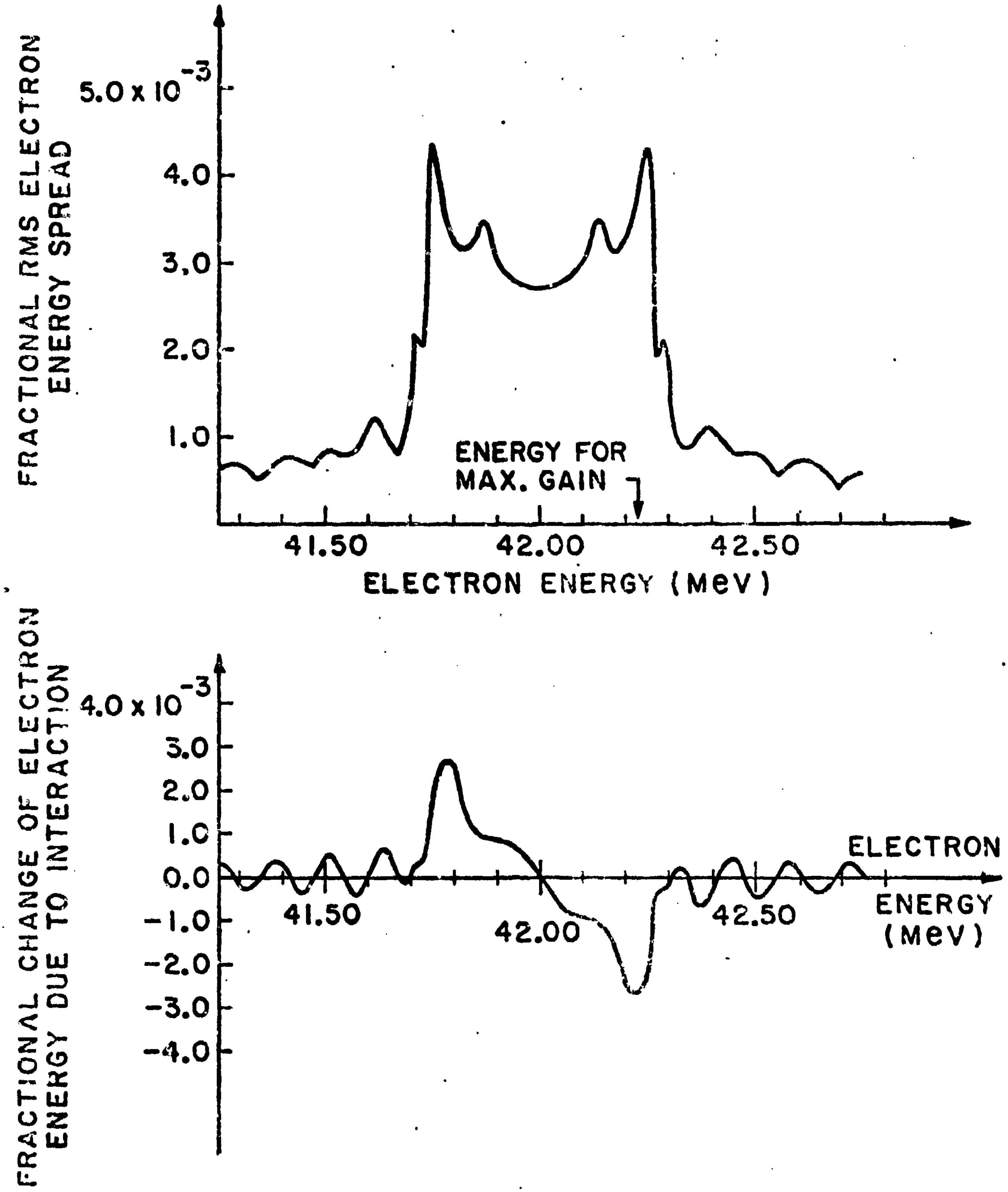

FRACTIONAL RMS ELECTRON ENERGY SPREAD
5.0 x 10^-3
4.0
3.0
2.0
1.0
ENERGY FOR MAX. GAIN
41.50
42.00
42.50
ELECTRON ENERGY (MeV)
FRACTIONAL CHANGE OF ELECTRON ENERGY DUE TO INTERACTION
4.0 x 10^-3
3.0
2.0
1.0
0.0
-1.0
-2.0
-3.0
-4.0
41.50
42.00
42.50
ELECTRON ENERGY (MeV)

Figure 3

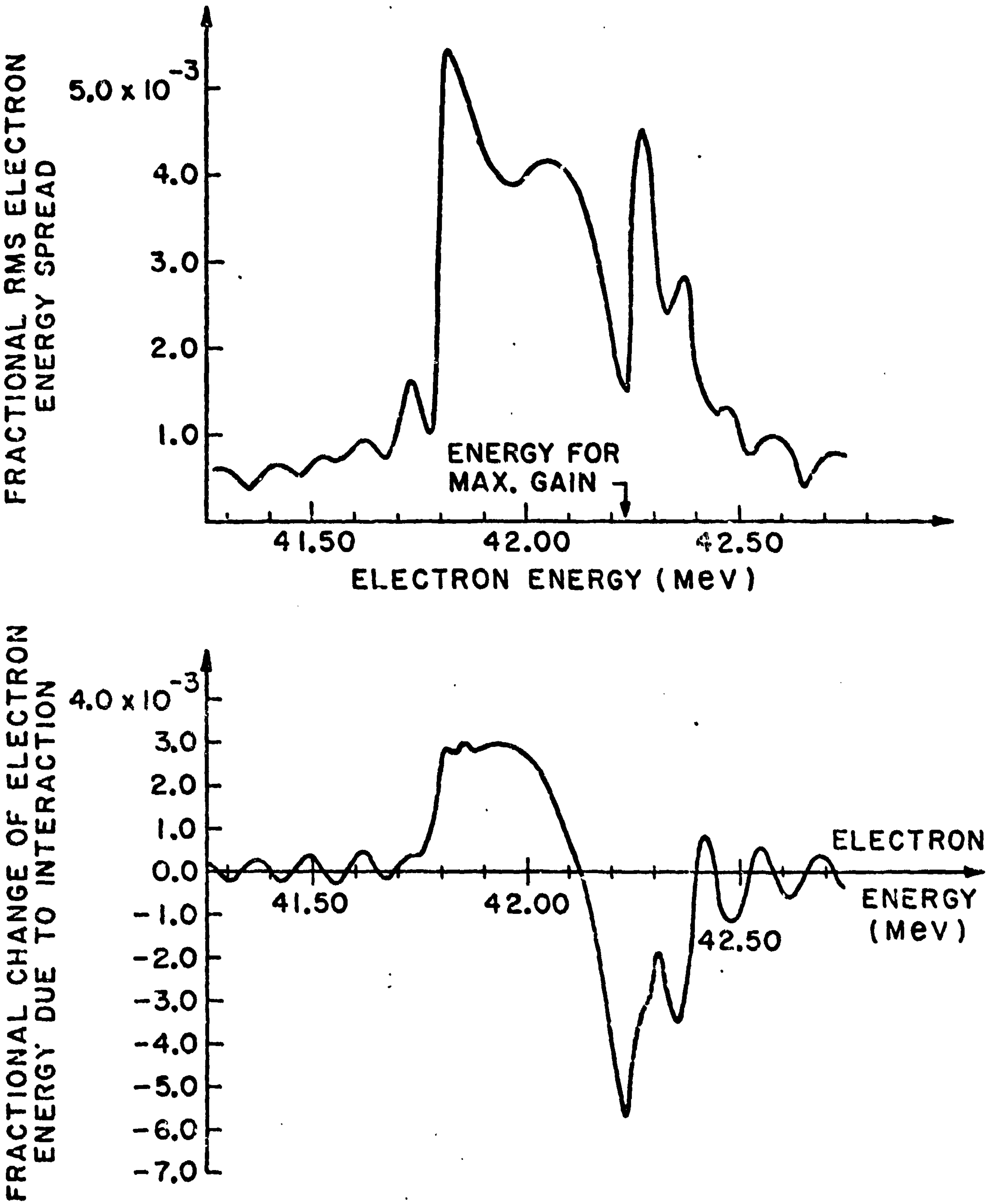
FRACTIONAL RMS ELECTRON
ENERGY SPREAD
5.0 x 10^-3
4.0
3.0
2.0
1.0
ENERGY FOR
MAX. GAIN
41.50
42.00
42.50
ELECTRON ENERGY (MeV)
FRACTIONAL CHANGE OF ELECTRON
ENERGY DUE TO INTERACTION
4.0 x 10^-3
3.0
2.0
1.0
0.0
-1.0
-2.0
-3.0
-4.0
-5.0
-6.0
-7.0
41.50
42.00
42.50
ELECTRON
ENERGY
(MeV)

Figure 4

HEPL 824
September 1978

ONE DIMENSIONAL MONTE CARLO ANALYSIS OF A FREE ELECTRON LASER IN A STORAGE RING*

L. R. Elias, J. M. J. Madey, and T. I. Smith

Department of Physics and High Energy Physics Laboratory
Stanford University, Stanford, California 94305

*Work supported in part by U.S. Army CMD-ATC, under Contract Number DASG 60-77-C-0083.

ONE DIMENSIONAL MONTE CARLO ANALYSIS OF A FREE ELECTRON LASER IN A STORAGE RING*

L. R. Elias, J. M. J. Madey, and T. I. Smith

Department of Physics and High Energy Physics Laboratory
Stanford University, Stanford, California 94305

ABSTRACT

We report the results of a montecarlo analysis of the equilibrium energy spread, bunch length, and average energy radiated by electrons in a storage ring free electron laser.

*Work supported in part by U.S. Army CMD-ATC, under Contract Number DASG 60-77-C-0083.

Introduction

The present report deals only with computer data obtained before February 15, 1978 and does not discuss the operations of the FEL in a storage ring when transverse field gradients (i.e., gain expansion) are allowed in the FEL magnet. A subsequent report will discuss these effects in detail.

This report contains studies of energy and phase dynamics of a single electron interacting with a free electron laser (FEL) oscillator operating in an electron storage ring. The studies include numerical integration of the energy and phase equations of motion to calculate equilibrium values of a) electron energy spread, b) electron phase spread (electron bunch length), and c) average electron energy converted into laser radiation. The non-equilibrium motion of the electron energy is analyzed by means of the energy autocorrelation function which yields, among other things, an effective damping rate for the electron energy motion. In addition, the energy autocorrelation function allows to qualitatively describe the mechanisms involved in the damping and excitation of electron energy oscillations and fluctuations. Storage ring simulations for five different magnet designs operating at optical power densities below saturation were studied. The results are presented here.

Description of the Problem

A complete discussion of the physics of electron storage rings can be found in reference 1. Figure 1 shows the three basic components of a FEL oscillator in a storage ring. There are: a) a free electron laser oscillator, b) a radio frequency cavity, and c) bending magnets.

78 10 16 02

The bending magnets guide the electrons into racetrack-type closed orbits whose lengths are proportional to the electron's energy. Two such orbits are shown in figure 1. Since the velocity of a relativistic electron is very close to the velocity of light, then the revolution time of the electron moving along one of its closed orbits is also proportional to the energy of the electron.

The FEL oscillator extracts energy from the circulating electron and converts it into laser radiation. To maintain equilibrium the energy lost by the electron is replaced by means of a radio frequency or microwave cavity. The amount of energy gained by the electron depends on its time of arrival to the RF cavity. The phase and frequency of the RF field in the cavity is adjusted to accelerate the early-arriving, low energy electrons more than the late-arriving, high energy electrons.

If the energy fluctuations resulting from the interaction of the electrons with the FEL oscillator were neglected, the problem of designing a FEL storage ring operating at high laser power and high efficiency would be considerably simplified. In equilibrium, the exact amount of energy lost by the electron to laser radiation would be exactly replaced by the RF cavity and the electron motion would be stable.

In a real FEL storage ring machine an electron may lose or gain energy from the FEL depending on the optical phase with which the electron enters the laser interaction region.

Although, in principle, the classical trajectory of an electron can be determined with arbitrary accuracy, in a real machine whose

dimensions are many optical wavelengths (typically > 10^7 λ) the position of the electron can be determined with only a limited precision. The assumption made in the present analysis is that the precision with which the electron position is determined at the entrance to the FEL is larger than one optical wavelength and as a result the phase with which the electron interacts with the optical wave in the FEL assumes random values uniformly distributed in the interval [0, 2π] on every pass. With this assumption the FEL behaves as a source of fluctuations in electron energy. However, averaged over input phases, the FEL also provides damping of energy fluctuations. If the damping rate of energy fluctuations generated by the FEL is always smaller than the rate at which it excites energy fluctuations, then the energy spread in the storage ring will grow without limit, making the efficient operation of a free electron laser in a storage ring virtually impossible.

The most important result presented in this port is that, for the FEL magnet designs studied in the storage ring simulations, the electron energy spread does not increase without limit. The FEL in conjunction with the other components of the storage ring is capable of damping the electron energy fluctuations that it produces, but the final equilibrium energy spread generated is as large as the energy of the FEL gain-absorption curve. As a result the FEL can operate in a storage ring only at reduced laser power and low efficiency.

The Free Electron Laser - Lineshape Simulations

The interaction of an electron with the Free Electron Laser can be described classically in terms of the work done by the electric field of the optical radiation on the electron as it moves through the FEL periodic static magnetic field.

Using the Lorentz force equations it is straightforward to show that the net change in energy $\delta\gamma$ (in units of mc^2) of an electron as it completes one pass through the FEL is given by:

$$\delta\gamma = \frac{q}{mc^2} \int_0^L \frac{\vec{E}_R \cdot \vec{V}}{V_z}\, dz \qquad (1)$$

where:

$\vec{E}_R$ = Electric field of optical radiation
$\vec{V}$ = electron velocity vector = $\hat{i}V_x + \hat{j}V_y + \hat{k}V_z$
L = length of interaction region.

For example, for a circularly plane polarized radiation field of wavelength λ and a helically wound magnet of period λ_M, equation (1) becomes

$$\delta\gamma = \frac{qE_R}{mc^2} \int_0^L \frac{V_\perp}{V_z} \cos(\theta)\, dz \qquad (2)$$

where

$$\theta = \theta_o + \frac{2\pi}{\lambda_M} \int_0^L \left[1 - \frac{\lambda_M}{\lambda}\left(\frac{c}{V_z} - 1\right)\right] dz \qquad (3)$$

and θ_o is the initial phase of the electron with respect to the optical radiation field.

For a monochromatic beam of electrons the energy transfer characteristics of a FEL oscillator may best be described in terms of its moments $\overline{\delta\gamma^n}$ averaged over initial phases:

$$\overline{\delta\gamma^n} = \frac{1}{2\pi}\int_{\theta_o=0}^{\theta_o=2\pi} (\delta\gamma)^n \, d\theta_o \quad . \tag{4}$$

Results of numerical integrations[2] $\overline{\delta\gamma}$ and $\overline{\delta\gamma^2}$ for the present Stanford FEL amplifier operating at an optical power density of $S = 10^5$ watts/cm^2 is shown in Figure 2. The figure shows the dependence of $\overline{\delta\gamma}$ and $(\overline{\delta\gamma^2})^{1/2}$ as a function of input electron energy measured with respect to the resonance energy. The resonance energy γ_R is defined as that input energy for which $\overline{\delta\gamma} = 0$. Analytically γ_R can be evaluated by letting the argument of the integral in eq. (3) be equal to zero and solving for V_z and subsequently for γ_R in terms of λ, λ_M and B_M. The result is

$$\gamma_R = \left[\frac{\lambda_M}{2\lambda} \left(1 + aB_M^2\right)\right]^{1/2} \tag{5}$$

where a is a geometric factor for the periodic magnet and B_M is the RMS magnetic flux density in the static periodic magnet. For $\gamma \gtrsim \gamma_R$, an electron on the average loses energy and as a result the EM wave is amplified. For $\gamma \lesssim \gamma_R$, the electron gains energy from the optical radiation field leading to the attenuation of the EM wave. Quantum mechanically, these two processes correspond to stimulated emission and absorption of radiation respectively.

Madey[3] has demonstrated that to lowest order in E_R, $\overline{\delta\gamma} =$

$\frac{1}{2}\frac{d\overline{\delta\gamma^2}}{d\gamma}$ and that there is a similarity in the functional dependence on energy of the second moment $\overline{\delta\gamma^2}$ and the spectral power density for spontaneous radiation.

These results have been used in the present analysis to generate electron energy transfer characteristics for five different magnets operating below saturation. With this approximation $\delta\gamma$ in eq. (2) can be written as follows:

$$\delta\gamma = \overline{\delta\gamma} + \sqrt{2}\,(\overline{\delta\gamma^2})^{1/2} \cos(\theta_o) \tag{6}$$

where $\overline{\delta\gamma} = \frac{1}{2}\frac{d\overline{\delta\gamma^2}}{d\gamma}$.

The analytic expressions describing the various spontaneous radiation lineshapes used in the storage ring simulations are listed on Table I.

All magnets were designed to have the same resonance energy $\gamma_R = 83.365$ and maximum mean electron energy loss at $\gamma = \gamma_R + 0.1$. In addition, the maximum value of $\overline{\delta\gamma^2}$ for each magnet was adjusted in such a way that

$$\int_{-\infty}^{\infty} (\overline{\delta\gamma})^2 \, d\gamma = KS \tag{7}$$

where K is a constant obtained by calculating (7) for the magnet used at the Stanford FEL experiment. S is the optical power density.

The dependence of $\overline{\delta\gamma}$ and $\overline{\delta\gamma^2}$ on input energy $(\gamma-\gamma_R)$ for the five lineshape simulations at $S = 10^5$ watts/cm^2 is shown in Figure

3. The magnet with a sin x/x lineshape approximates quite well the present magnet used at Stanford and whose energy transfer characteristics are illustrated in Figure 2.

<u>Equations of Motion</u>

If the energy γ_n of the electron is measured at point A (see Fig. 1) just before the FEL oscillator, then after one complete revolution moving counterclockwise, the energy γ_{n+1} is given by

$$\gamma_{n+1} = \gamma_n + \delta\gamma(\gamma_n, \theta_n) + V \cos\left[\frac{2\pi}{T}(\tau_n + \tau_S)\right] - 2\,\frac{(\gamma_{n+1} - \gamma_S)}{N_S} \quad (8)$$

where $\delta\gamma(\gamma_n, \theta_n)$, given by either eqs. (2) or (6), is the energy (measured in units of mc^2) gained by the electron from the FEL oscillator. $\delta\gamma$ depends on the initial electron energy and initial optical phase θ_r.

The third term on the right hand side of eq. (8) represents the energy gained by the electron in the RF cavity. The energy gained depends on the time of arrival $\tau_n + \tau_S$ of the electron at the RF cavity. Here τ_n is the time distance between the arrival of the electron and the arrival of an ideal synchronous electron. The energy γ_S and phase τ_S of the synchronous electron is defined in the following way. Moving counterclockwise in Figure 1 from point C to point B, the synchronous electron with energy γ_S at C will arrive at point C, just before the RF cavity, at a time τ_S such that the energy gained from the RF cavity is equal to the average equilibrium energy $\overline{\Delta\gamma}$ lost to the FEL radiator. From eq. (1) at

equilibrium $\overline{\gamma_{n+1}} = \overline{\gamma_n}$ and

$$\tau_S = \frac{T}{2\pi}\cos^{-1}\frac{\overline{\Delta\gamma}}{V}$$

where T is the period of the RF field and V is the maximum energy that the electron can gain from the RF cavity.

The last term on the RHS of eq. (8) describes the damping effect that synchrotron radiation has on the electron energy. In all of the storage ring simulation, it has been assumed that N_S = 50,000 turns.

The reference trajectory of the electron is assumed to be the ideal trajectory of the synchronous electron. With respect to this trajectory the fractional change in orbit length (revolution time) is proportional to the fractional electron energy deviation from the ideal synchronous energy. The proportionality constant α, named by M. Sands[1] the dilation factor, is defined as

$$\alpha = \frac{\Delta t/T}{(\gamma - \gamma_S)/\gamma_S} .$$

The change in time position τ in one pass through the storage is then given by

$$\tau_{n+1} = \tau_n + \alpha T\,\frac{(\gamma_{n+1} - \gamma_S)}{\gamma_S} . \quad (9)$$

If the energy of the electron is measured with respect to the synchronous energy ($\Delta\gamma = \gamma - \gamma_S$), then the two coupled equations

describing the evolution of phase and energy of an electron in a FEL storage ring are as follows:

$$\Delta\gamma_{n+1} = \Delta\gamma_n - 2\frac{\Delta\gamma_n}{N_S} + \delta\gamma(\Delta\gamma_n, \theta_n) + V\cos\left[\frac{2\pi}{T}(\tau_n - \tau_S)\right] \qquad (10)$$

$$\tau_{n+1} = \tau_n + \frac{\alpha T}{\gamma_S}\Delta\gamma_{n+1} \quad . \qquad (11)$$

The above non-linear equations of motion have been linearized and studied in detail by M. Sands[4] for a gaussian lineshape simulation.

Numerical Results

The full nonlinear equations of motion (10) and (11) were integrated numerically for the magnet lineshapes shown in Figure 3 and for various ranges of optical power density S, dilation factor α, maximum energy gained from the RF cavity V, and synchronous energy γ_R. The most important results are listed in Table II.

All the simulations were made for $N = 100{,}000$ revolutions of the electron in the storage ring. A random number generator program written by G. Marsaglia, et al., from McGill University was used to initialize the optical phase of the electron on every turn just before interacting with the FEL.

After 100,000 revolutions in the storage ring simulation program, the performance of the various magnet lineshapes was evaluated in terms of the following quantities:

a) Equilibrium RMS spread σ of electron energy just before the FEL magnet

$$\sigma^2 = \frac{1}{N-1}\sum_{J=1}^{N}(\Delta\gamma_J - \overline{\Delta\gamma})^2$$

where N is the number of passes in the storage ring and

$$\overline{\Delta\gamma} = \frac{1}{N}\sum_{J=1}^{N}\Delta\gamma_J = \frac{1}{N}\sum_{J=1}^{N}(\gamma_J - \gamma_S)$$

is the equilibrium mean value of the energy measured with respect to the synchronous energy just before the FEL.

For all magnet lineshapes, σ had very little dependence on V and α over the ranges of $0.01 \to 0.11$ and $0.02 \to 0.1$ respectively. Increasing the optical power density from $S = 10^4$ watts/cm^2 to $S = 10^5$ watts/cm^2 did not increase the equilibrium spread σ by more than a factor of 2. However there is a strong dependence of σ on γ_S as shown in Figure 4 for the gaussian lineshape simulation at $S = 10^5$ watts/cm^2.

The minimum energy spread occurs for $\gamma_S = \gamma_R$ and it increases monotonically for $\gamma_S > \gamma_R$. The apparent leveling-off of σ at $\gamma_S - \gamma_R = 0.4$ is an indication that the total number of passes $N = 100{,}000$ were not sufficient to generate an equilibrium value for σ. However, the effective damping time N_D has increased abruptly indicating that the energy and phase oscillations are still increasing and equilibrium has not been reached.

One general conclusion about σ for the magnet lineshapes analyzed is that the minimum attainable equilibrium value of σ

is <u>always</u> as large, or larger than the gain-absorption width of the magnet lineshape.

b) Mean energy $\overline{\Delta\Gamma}$ lost by the electron to the FEL:

$$\overline{\Delta\Gamma} = \frac{1}{N} \sum_{J}^{N} (\gamma_J{}^B - \gamma_J{}^A)$$

where $\gamma_J{}^A$ and $\gamma_J{}^B$ are defined as the energy of the electron just before and just after the FEL (see Figure 1) respectively during the J^{th} pass of the electron in the storage ring simulation. $\overline{\Delta\Gamma}$ is, of course, the mean energy gained per electron by the radiation field in the FEL optical cavity. The average power converted into radiation by a beam of electrons is $\overline{\Delta\Gamma}\ mc^2\ (I/e)$ where I is the average electron current in the storage ring.

$\overline{\Delta\Gamma}$ showed approximately the same behavior as σ as a function of α, V and S. The maximum amount of average energy $\overline{\Delta\Gamma}(\gamma_{SM})$ that could be extracted from the electron occurred for values of γ_S somewhere in the range between γ_R and $\gamma_R + 0.1$ depending on the particular FEL magnet design. The ranges of maximum output laser power varied from a minimum value of 7.5 watts/ampere for the parabolic lineshape simulation to 25 watts/ampere for the sin x/x lineshape simulation.

c) Equilibrium RMS time spread τ_{RMS}

$$\tau_{RMS}^2 = \frac{1}{N-1} \sum_{J=1}^{J=N} (\tau_J - \overline{\tau})^2$$

$$\overline{\tau} = \frac{1}{N} \sum_{J=1}^{J=N} \tau_J \ .$$

τ_{RMS} represents the time length of the electron bunch in the storage ring. For all lineshape simulations τ_{RMS} increased with α, decreased with V and increased with γ_S as shown in Figure 5. The period of the RF field was chosen to be $T = 40 \times 10^{-9}$ sec. The ranges of final equilibrium bunch lengths in the storage ring were from a maximum of 18° to a minimum of 1°.

d) Energy damping N_D

The discrete energy autocorrelation functions $\{A_K\}$ was evaluated as follows:

$$A_K = \sum_{J=0}^{M} \Delta\gamma_J\ \Delta\gamma_{J-K}$$

where M is the number of equally spaced samples of the energy $\Delta\gamma$ of the electron for one complete simulation record of 100,000 passes. The value of $\Delta\gamma$ was sampled every 100 revolutions yielding a total number of samples M = 1000. All the coefficients $\{A_K\}$ of the energy autocorrelation functions were plotted and an effective damping time N_D was graphically estimated for all storage ring simulations.

To understand the dynamic processes involved in generating the equilibrium energy and phase distributions of the electron, it is convenient to divide the energy domain accessible to the electron into two regions: a) the synchrotron radiation damping region and b) the FEL damping region. Figure 6 shows a plot of the derivative $\frac{d\delta\overline{\gamma}}{d\gamma}$ as a function of $(\gamma-\gamma_R)$ for the Stanford FEL magnet shown in Figure 2. $\frac{d\delta\overline{\gamma}}{d\gamma}$ is identified as the negative

of the average electron energy damping rate. Maximum damping rate occurs when the electron energy is near the resonance energy $\gamma - \gamma_R = 0$ of the FEL magnet. The damping rate decreases for $\gamma - \gamma_R > 0$ and becomes negative (antidamping) for $|\gamma - \gamma_R| > 0.1$. Beyond $|\gamma - \gamma_R| > 0.3$, the dominant damping mechanism is synchrotron radiation. The value of $\frac{d\delta\overline{\gamma}}{d\gamma}$ for synchrotron radiation is $\frac{d\delta\overline{\gamma}}{d\gamma} = - 1/N_D = - 2 \times 10^{-5}$ and is shown as a broken line in Figure 6.

In addition to damping energy oscillations the FEL excites random electron energy fluctuations resulting from the random values of optical phase with which the electron enters the interaction region. The spread of the fluctuations $(\overline{\delta\gamma^2})^{1/2}$ are shown in Figure 2 as a function of input energy γ-γ_R.

Equilibrium in the storage ring is reached when the rate at which random energy fluctuations generated by the FEL equals the rate at which the energy fluctuations are damped by the FEL and by synchrotron radiation.

A typical simulation of energy and phase evolution in an FEL storage ring is illustrated in Figure 7. The black dots represent the energy of the electron and the solid triangles represent the phase of the electrons as a function of the revolution number in the simulation. The two figures shown illustrate qualitatively how synchrotron radiation energy damping and energy damping from the FEL contribute to decrease the amplitude of the large synchrotron oscillations. The upper figure describes the evolution of the electron energy and phase for the first 1200 revolutions. The maximum energy excursion by the electron is about γ-γ_S = ± 0.8. The two horizontal dotted lines

shown above and below the synchronous energy bound the region of FEL positive energy damping. The energy and phase oscillate in a nearly perfect sinusoidal motion. However, there is a slow attentuation of the oscillations originating from synchrotron radiation damping (N_S = 50,000 turns). Both the average energy damping rate and energy fluctuations excitation rate by the FEL make a negligible contribution to the energy and phase motion of the electron during the first 10,000 turns. Even though the electron is swept through the energy interaction region of the FEL during each synchrotron oscillation the changes in energy produced by the RF cavity are too large and as a result the number of revolutions that the electron spends within the damping region of the FEL is too small compared to the total number of revolutions required to complete one synchrotron oscillation.

After the large synchrotron oscillations are damped by synchrotron radiation to amplitudes comparable to the energy width of the FEL interaction region the electron spends a larger portion of the synchrotron oscillation in the positive damping region of the FEL. As a result, the energy motion is more effectively damped by the FEL. The lower trace in Figure 7 illustrates this effect. After 11,400 passes the amplitude of the synchrotron oscillation is decreasing at a much faster rate than that shown in the upper trace. Also, when the same system was initialized close ot its synchronous condition ($\gamma = \gamma_S$, τ = 0) the energy and phase oscillations grew from zero amplitude to its final equilibrium values after approximately 1200 passes. Almost identical results were obtained when the FEL energy transfer characteristics were computed using Eqs. (2) and

(3) or when using the small signal approximation of Eq. (6).

When the damping term $\overline{\delta\gamma}$ in Eq. (6) was set to zero the system was not able to reach equilibrium in 100,000 passes. In fact, the ability of the system to reach equilibrium was tested for various non real relative ratios of $\overline{\delta\gamma}$ to $(\overline{\delta\gamma^2})^{1/2}$ in Eqs. (6). The results indicated that the equilibrium configurations of the system was very sensitive to this ratio. For example, increasing the value of the damping term $\overline{\delta\gamma}$ by a factor of 2 resulted in a final equilibrium energy spread smaller than 1/2 the width of the gain curve, with the electron almost completely constrained to have energies within the linear region of the gain curve, and as a consequence of this the final equilibrium state was approached at a much faster rate than in the real case ($N_D < 500$ passes).

The triangular lineshape simulation was the most effective in damping energy oscillations (N_D = 3300 revolutions at $S = 10^5$ watts/cm^2). At $S = 10^4$ watts/cm^2 the Lorentzian lineshape showed the least amount of energy damping ($N_D > 25{,}000$ revolutions). This was expected, since the maximum slope of the Lorentzian lineshape gain curve has the smallest value of all the magnet lineshapes studied.

The dependence of energy damping $1/N_D$ on synchronous energy γ_S is shown in Figure 4 for the sin (x)/x lineshape simulation. As the value of $(\gamma_S - \gamma_R)$ increases beyond the width of the FEL $\overline{\delta\gamma}$ - VS - $(\gamma - \gamma_R)$ curve the damping rate $1/N_D$ decreases and becomes nearly equal to the synchrotron damping rate $\frac{1}{N_S} = \frac{2 \times 10^{-5}}{\text{REV}}$ at

$(\gamma_S - \gamma_R) = 0.45$. This result is in agreement with the previously discussed picture where the damping of electron energy by the FEL is very small when the energy amplitude of synchrotron oscillations is larger than the energy width of the gain curve.

Conclusions

The results presented here indicate that the simple FEL magnet lineshapes studied in a storage ring do not provide efficient conversion of electron kinetic energy to laser radiation. The largest expected average power attainable from a storage ring FEL laser is of the order of tens of watts per ampere of stored electron beam current.

Research work is underway at Stanford University to study other magnet designs which will hopefully increase the operating efficiency of a free electron laser in a storage ring.

LIST OF IMPORTANT SYMBOLS

γ = electron energy measured in units of mc^2.

γ_S = synchronous electron energy.

γ_R = resonance electron energy.

$\delta\gamma$ = energy absorbed by electron from the FEL optical radiation field in units of mc^2,

$\Delta\gamma$ = energy of electron in a storage ring measured with respect to the synchronous energy in units of mc^2.

V = maximum increase in electron energy from the radio frequency cavity in units of mc^2.

τ = time distance (in seconds) between electron and synchronous electron just before entering RF cavity.

τ_S = time of arrival (in seconds) of synchronous electron at RF cavity.

T = period (in seconds) of RF field.

θ = optical phase (in degrees) of electron.

N = total number of revolutions of the electron in the storage ring.

N_S = synchrotron radiation energy damping time measured in number of revolutions.

N_D = effective energy damping time of electron in FEL storage ring measured in number of revolutions.

α = dilation factor.

σ = equilibrium root mean square deviations (in units of mc^2) of electron energy from the mean in the FEL storage ring.

$\overline{\Delta\gamma}$ = equilibrium mean energy (in units of mc^2) lost by electron to the FEL radiation field.

S = FEL optical power density in units of watts/cm^2.

λ = wavelength (in meters) of optical radiation field.

λ_M = wavelength (in meters) of FEL periodic magnetic field.

B_M = RMS magnetic flux density in FEL periodic magnet in units of weber/m^2.

REFERENCES

1. M. Sands, The Physics of Storage Rings, Stanford Linear Accelerator Center, Report No. 121 (1970).
2. J. M. J. Madey, D. A. G. Deacon, L. R. Elias, and T. I. Smith, "An approximate technique for the integration of the equation of motion in a Free Electron Laser," to be submitted for publication to Physical Review.
3. J. M. J. Madey, "Relationship between mean radiated energy, mean squared radiated energy, and spontaneous power spectrum in a power series expansion of the equations of motion in a free electron laser," Stanford University High Energy Physics Laboratory, Report No. 823 (1978).
4. M. Sands, Storage-Ring-Laser, Laboratori Nazionali di Frascati del C.N.E.N. Internal Memorandum (1975).

FIGURE CAPTIONS

Fig. 1. Diagram of basic components of a free electron laser in a storage ring.

Fig. 2. Energy dependence of $\overline{\delta\gamma}$ and $(\overline{\delta\gamma^2})^{1/2}$ below saturation for the Stanford University FEL magnet.

Fig. 3. Energy dependence of $\overline{\delta\gamma}$ and $\overline{\delta\gamma^2}$ for five different FEL magnet designs operating below saturation at $S = 10^5$ watts/cm^2.

Fig. 4. Dependence of equilibrium RMS spread σ and effective energy damping constant $1/N_D$ on synchronous energy for the guassian lineshape simulation at $S = 10^5$ watts/cm^2.

Fig. 5. Dependence of equilibrium electron bunch length τ_{RMS} on RF cavity maximum electron energy gain V.

Fig. 6. The solid line shows the energy dependence of the FEL damping rate $-\frac{d\overline{\delta\gamma}}{d\gamma}$ for the magnet shown in Fig. 1. The broken line shows the energy dependence of the damping rate $2/N_S = -\frac{d\overline{\delta\gamma}}{d\gamma}$ for synchrotron radiation.

Fig. 7. Typical energy and phase record for an electron in a FEL storage ring showing the damping of synchrotron oscillations during the first 1200 passes (top figures) and the damping of energy and phase oscillations by the FEL after 11,400 revolutions. The horizontal broken lines bound the positive damping region of the FEL.

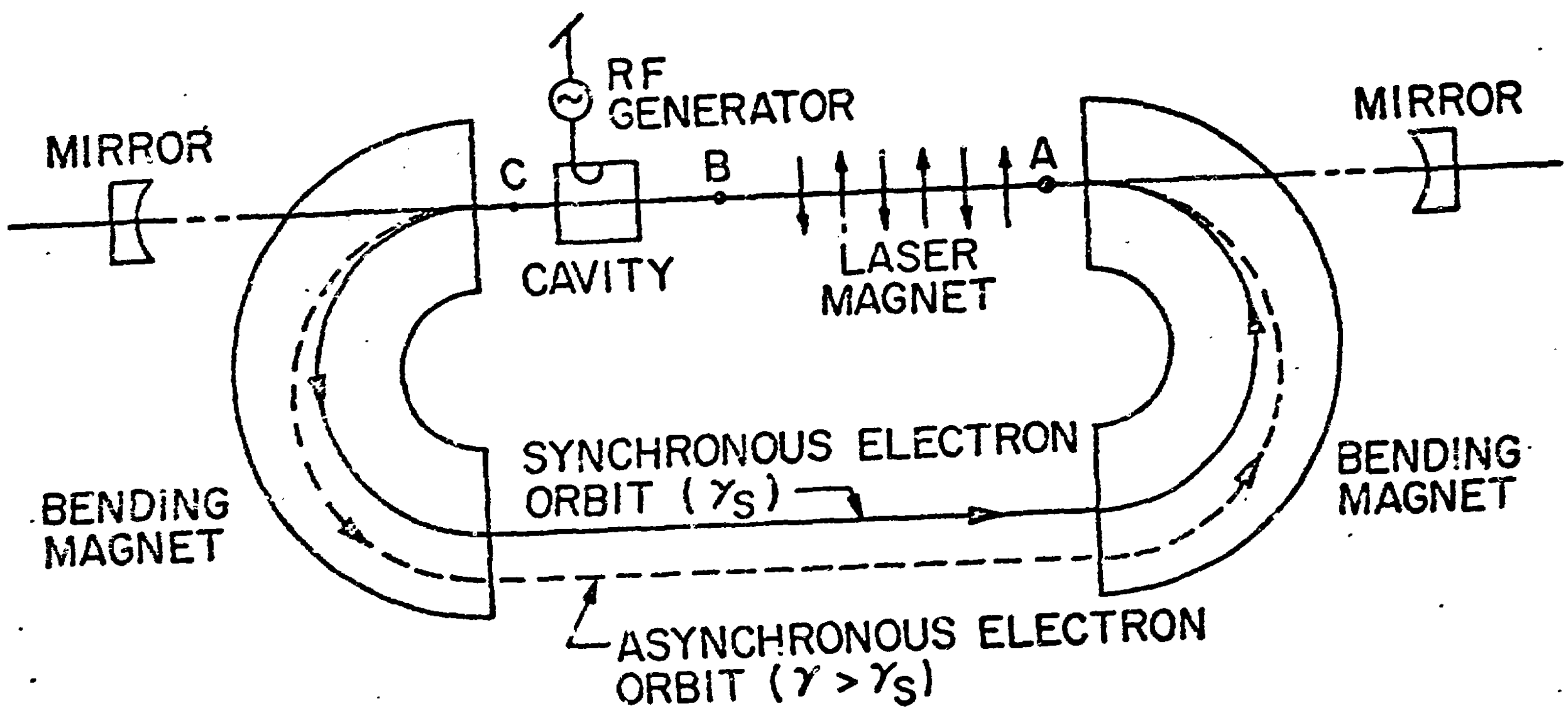
RF GENERATOR
MIRROR
MIRROR
C
B
A
CAVITY
LASER MAGNET
SYNCHRONOUS ELECTRON ORBIT (γ_S)
BENDING MAGNET
BENDING MAGNET
ASYNCHRONOUS ELECTRON ORBIT ($\gamma > \gamma_S$)

Figure 1

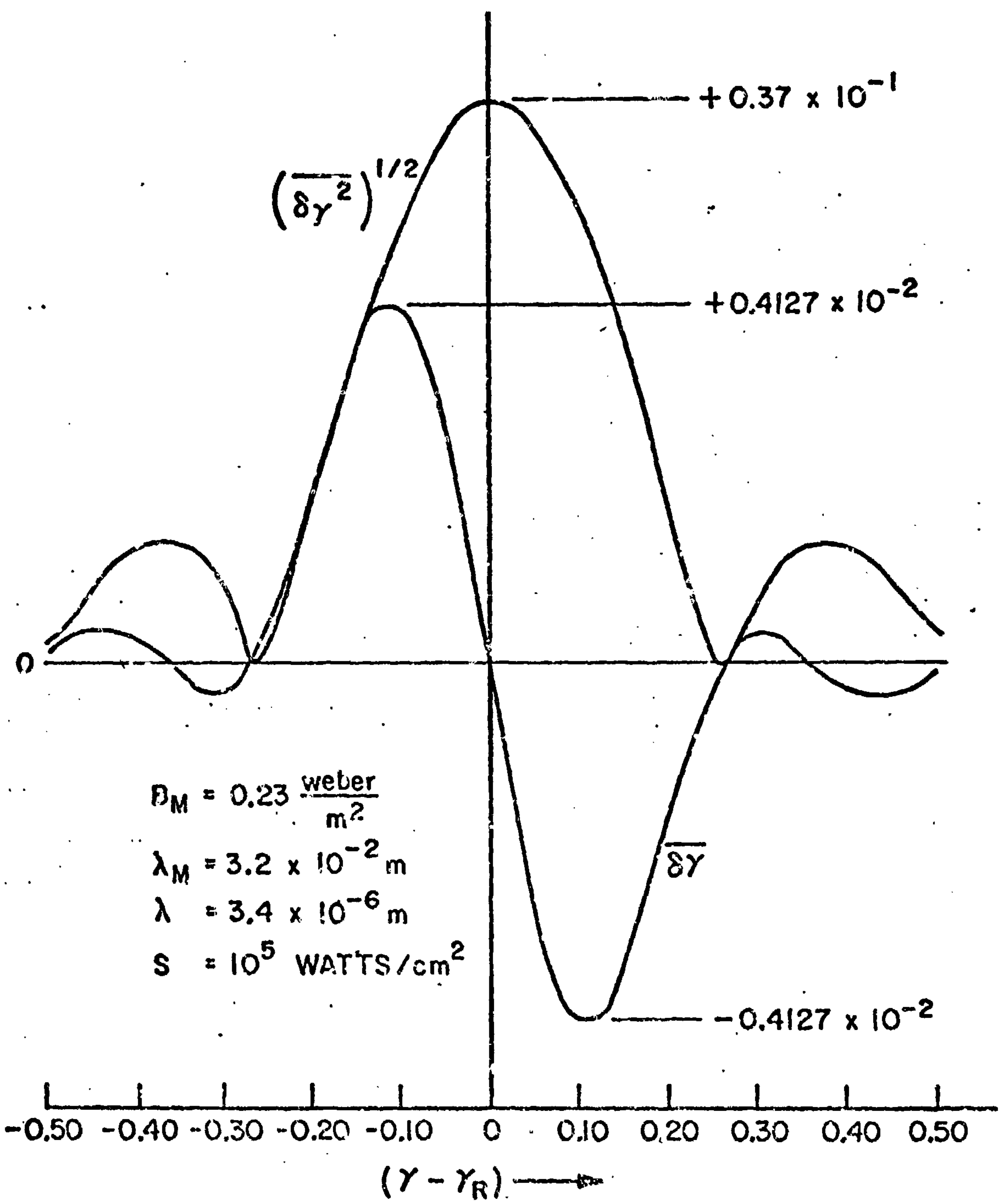
+0.37 x 10^-1
(δγ²)^1/2
+0.4127 x 10^-2
0
B_M = 0.23 weber/m²
λ_M = 3.2 x 10^-2 m
λ = 3.4 x 10^-6 m
S = 10^5 WATTS/cm²
δγ
-0.4127 x 10^-2
-0.50 -0.40 -0.30 -0.20 -0.10 0 0.10 0.20 0.30 0.40 0.50
(γ - γ_R)

Figure 2

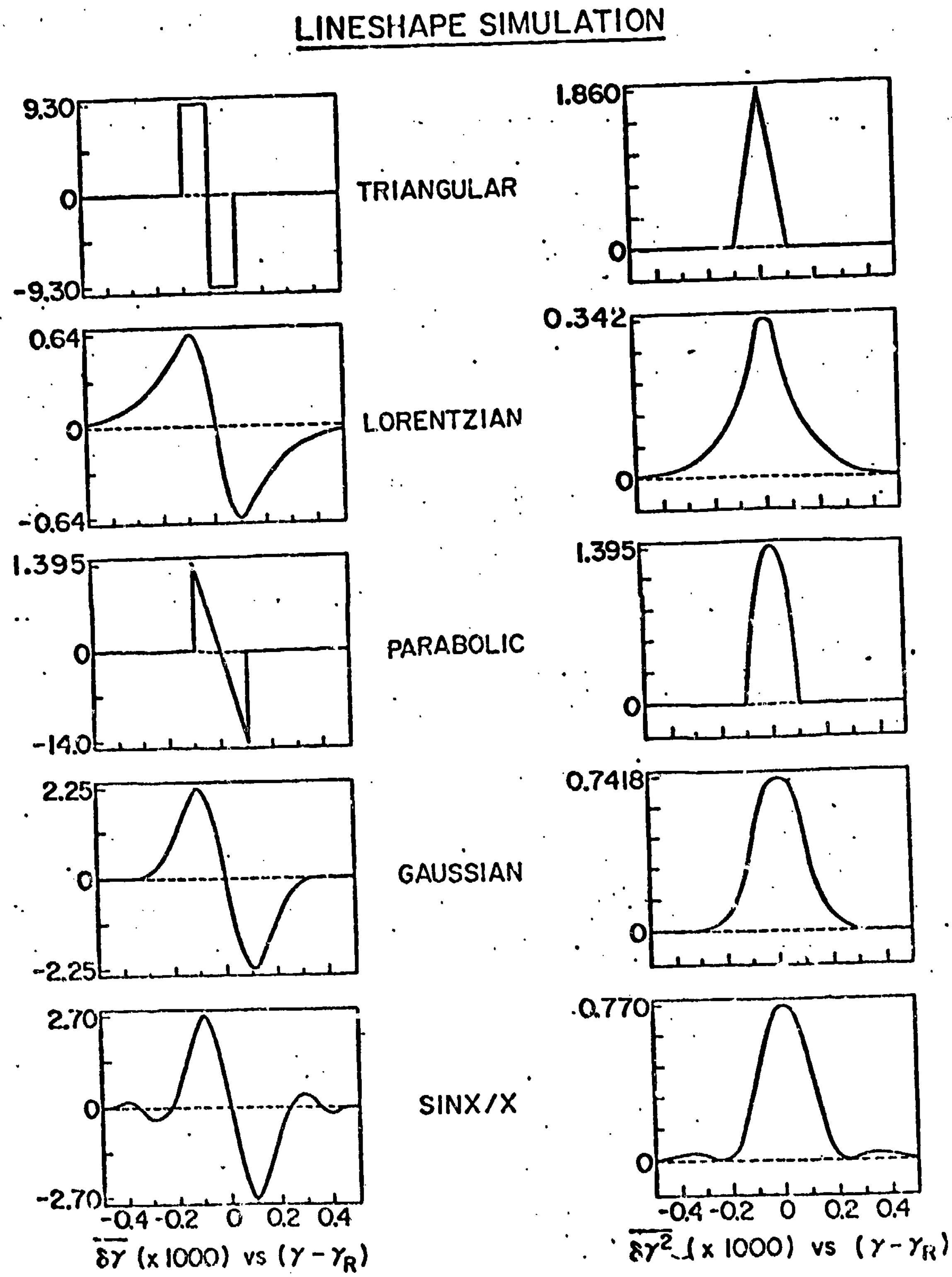
LINESHAPE SIMULATION
9.30
0
-9.30
TRIANGULAR
1.860
0
0.64
0
-0.64
LORENTZIAN
0.342
0
1.395
0
-14.0
PARABOLIC
1.395
0
2.25
0
-2.25
GAUSSIAN
0.7418
0
2.70
0
-2.70
SINX/X
0.770
0
-0.4 -0.2 0 0.2 0.4
δγ (x 1000) vs (γ - γR)
-0.4 -0.2 0 0.2 0.4
δγ2 (x 1000) vs (γ - γR)

Figure 3

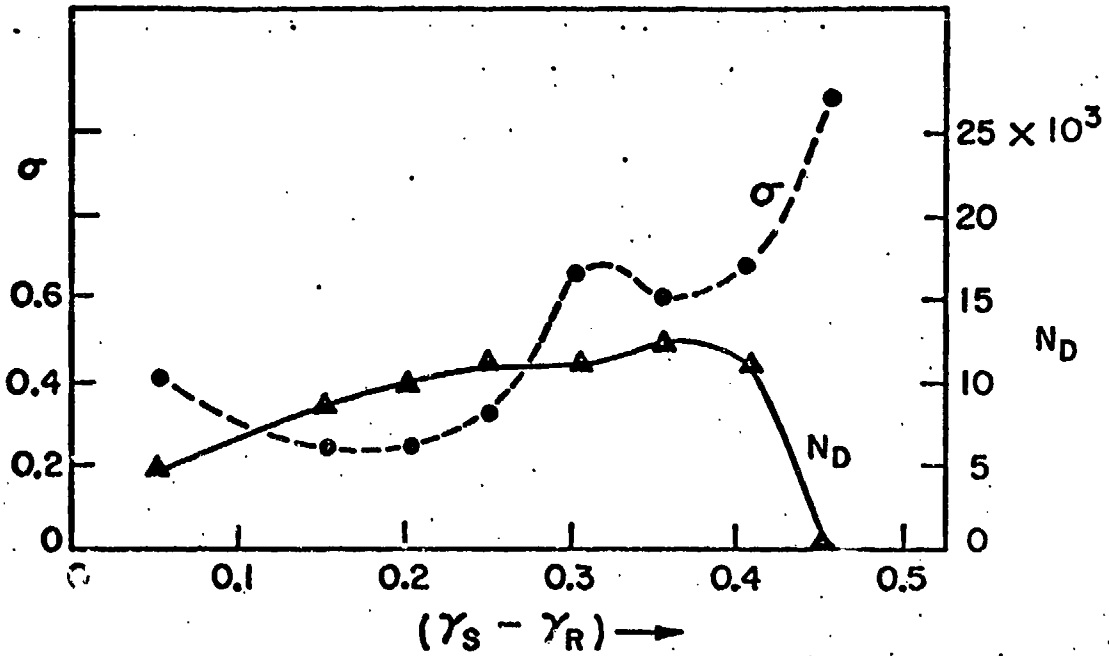

Figure 4

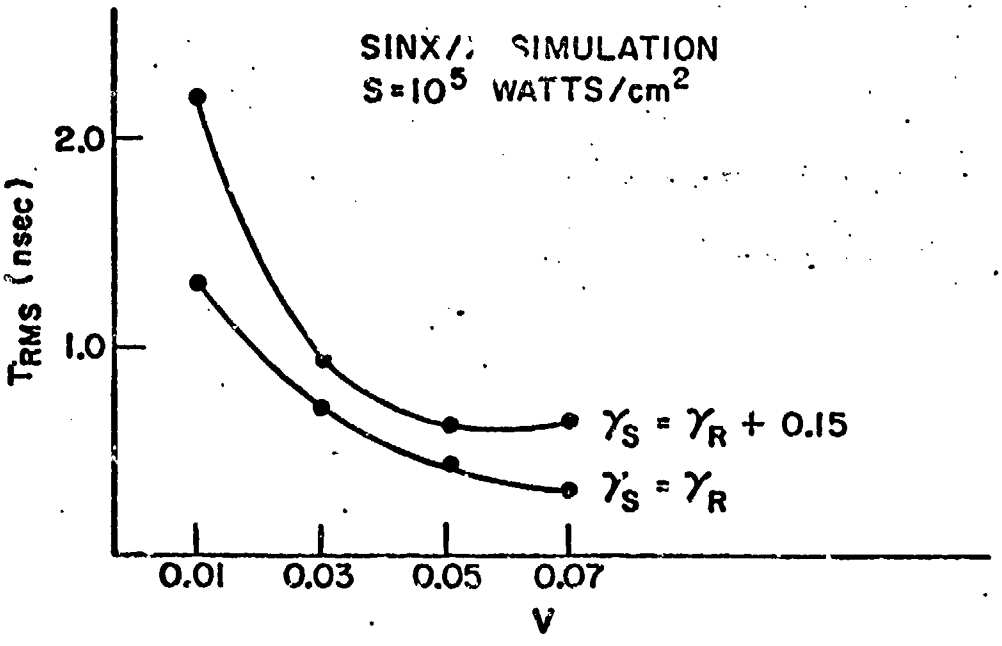

Figure 5

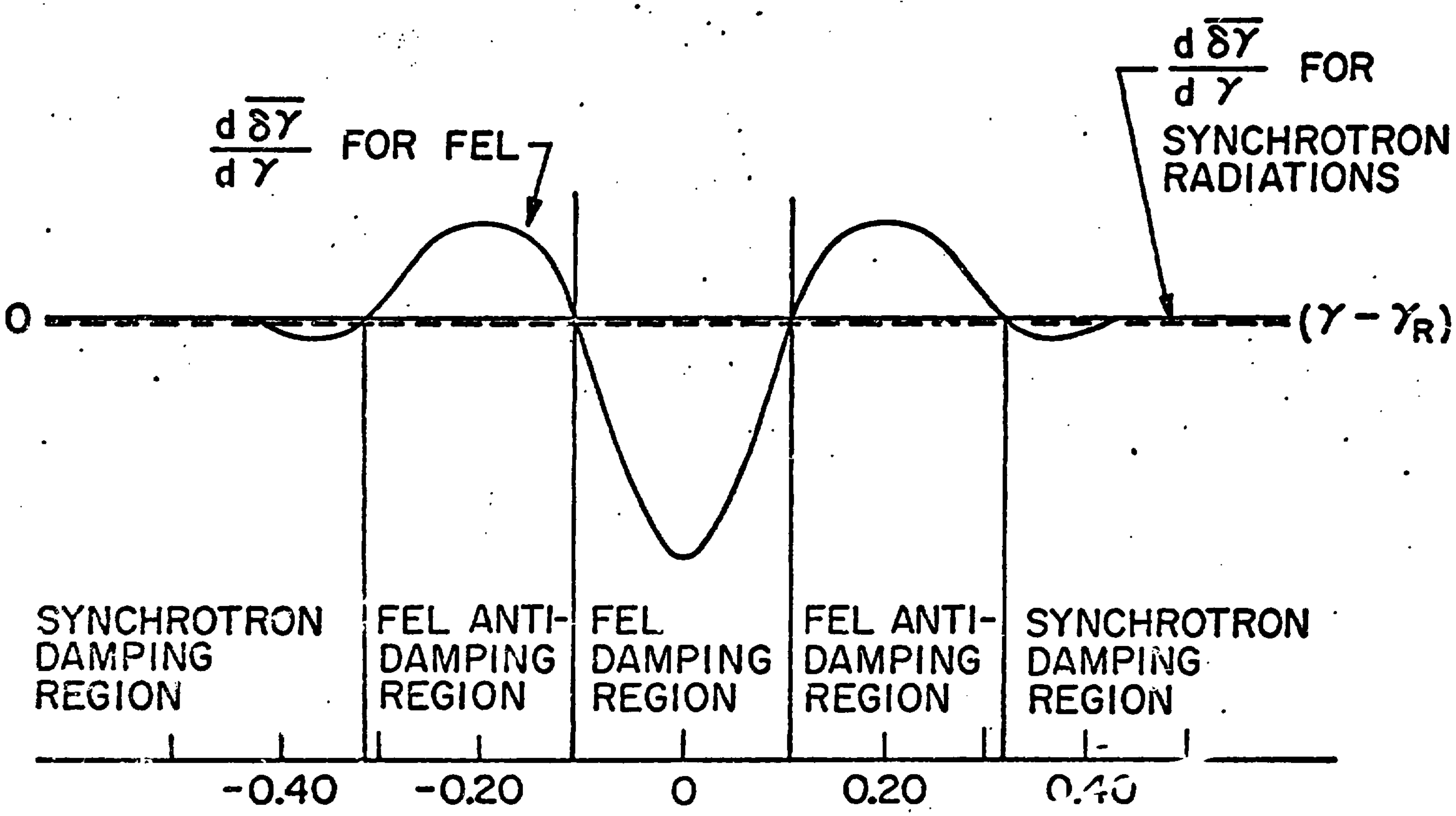

$\frac{d\overline{\delta\gamma}}{d\gamma}$ FOR FEL
$\frac{d\overline{\delta\gamma}}{d\gamma}$ FOR SYNCHROTRON RADIATIONS
0
$(\gamma - \gamma_R)$
SYNCHROTRON DAMPING REGION
FEL ANTI-DAMPING REGION
FEL DAMPING REGION
FEL ANTI-DAMPING REGION
SYNCHROTRON DAMPING REGION
-0.40
-0.20
0
0.20
0.40

Figure 6

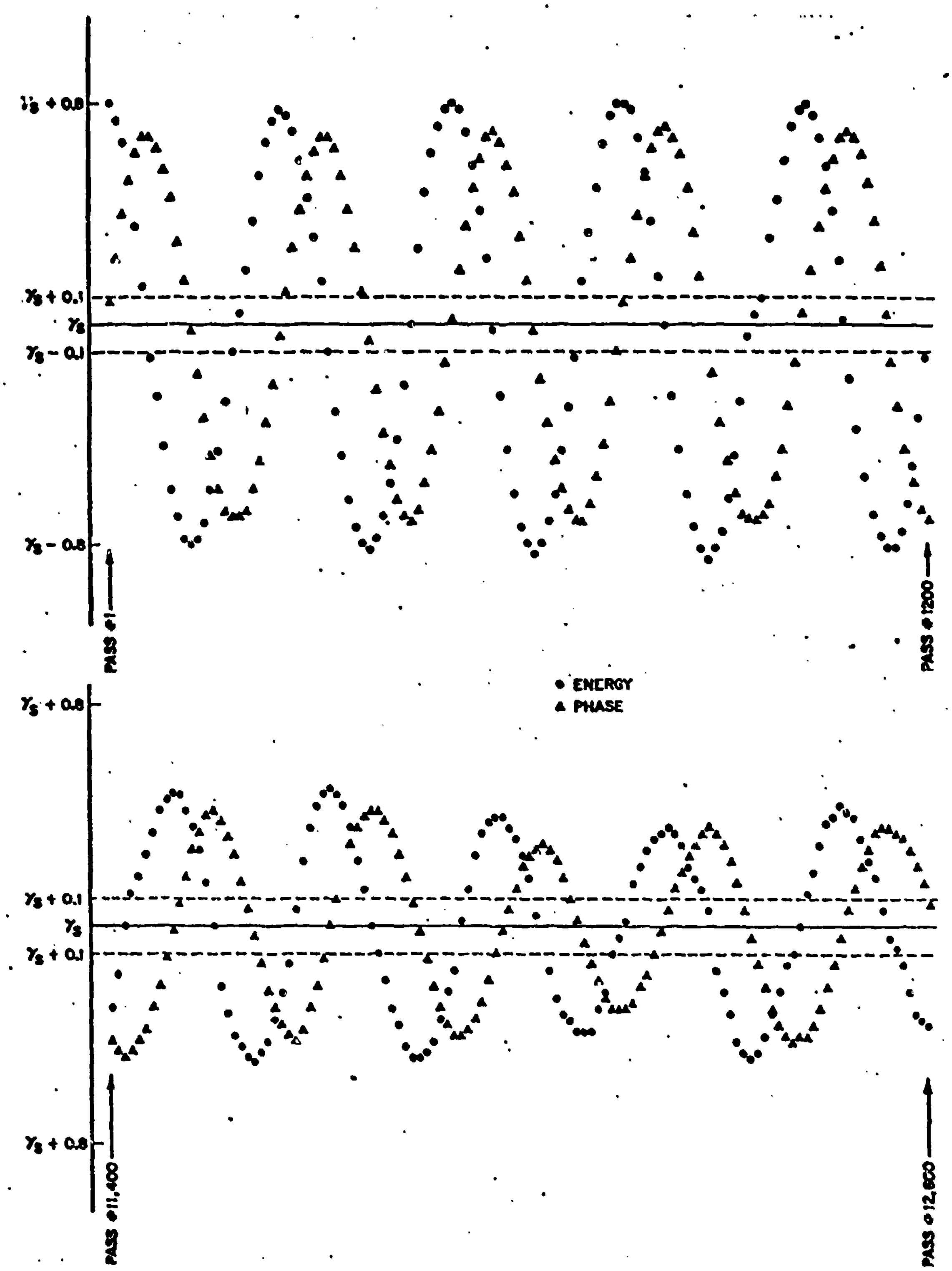

$\gamma_s + 0.8$
$\gamma_s + 0.1$
γ_s
$\gamma_s - 0.1$
$\gamma_s - 0.8$
PASS #1
PASS # 1200
• ENERGY
▲ PHASE
$\gamma_s + 0.8$
$\gamma_s + 0.1$
γ_s
$\gamma_s + 0.1$
$\gamma_s + 0.8$
PASS # 11,400
PASS # 12,600

Figure 7

TABLE I. ANALYTIC FORM OF SPONTANEOUS LINESHAPE SIMULATIONS

Lineshape $x = (\gamma-\gamma_R)/\Delta$	Δ	$\overline{\delta\gamma^2}$ †	$\overline{\delta\gamma}$	
Triangular	0.1	$\frac{K}{\Delta}[1-x]$	$-\frac{K}{2\Delta^2}$	$0 < x < 1$
		$\frac{K}{\Delta}[1+x]$	$\frac{K}{2\Delta^2}$	$-1 < x < 0$
		0	0	$\lvert x\rvert > 1$
Lorentzian	$\frac{\sqrt{3}}{10}$	$\frac{K}{\pi\Delta(1+x^2)}$	$-\frac{KX}{\pi\Delta^2(1+x^2)^2}$	$\lvert x\rvert < \infty$
Parabolic	0.1	$\frac{3K(1-x^2)}{4\Delta}$	$\frac{3KX}{4\Delta^2}$	$\lvert x\rvert < 1$
		0	0	$\lvert x\rvert > 0$
Gaussian	$\frac{\sqrt{2}}{10}$	$\frac{Ke^{-x^2}}{\sqrt{\pi}\,\Delta}$	$-\frac{K\,x\,e^{-x^2}}{\sqrt{\pi}\,\Delta^2}$	$\lvert x\rvert < \infty$
Sin x/x	$\frac{.1}{1.303}$	$\frac{K}{\pi\Delta}\sin^2(x)$	$\frac{K}{\pi\Delta^2}\frac{\sin(x)}{x^2}\left(\cos(x)-\frac{\sin(x)}{x}\right)$	$\lvert x\rvert < \infty$

† $K = 1.86 \times 10^{-9}$ S, where S is the optical power density in watts/cm^2.

TABLE II

Magnet Lineshape	γ_{SM} †	σ ††	$\overline{\delta\Gamma}$ (γ_{SM})	N_D
$S = 10^4$ watts/cm^2			$(\times 10^4)$	$(\times 10^{-3})$
Gaussian	83.565	0.260 ± 0.020	0.15 ± 0.06	24 ± 15
Parabolic	83.465	0.196 ± 0.017	0.16 ± 0.04	10 ± 1.6
Lorentzian	83.715	0.306 ± 0.050	0.13 ± 0.10	32 ± 13
sin x/x	83.415	0.250 ± 0.060	0.20 ± 0.20	16 ± 8
Triangular	83.415	0.195 ± 0.008	0.215 ± 0.46	7.8 ± 2.6
$S = 10^5$ watts/cm^2				
Gaussian	83.565	0.404 ± 0.03	0.30 ± 0.05	6.8 ± 2.5
Parabolic	83.445	0.266 ± 0.04	0.153 ± 0.149	8.5 ± 5
sin x/x	83.415	0.422 ± 0.07	0.46 ± 0.23	9.2 ± 2
Triangular	83.425	0.248 ± 0.06	0.38 ± 0.15	3.3 ± 1.4

† γ_{SM} is the value of synchronous energy for which maximum optical power output $\overline{\delta\Gamma}$ (γ_{SM}) was obtained.

†† σ is defined as $(\overline{\Delta\gamma^2} - \overline{\Delta\gamma}^2)^{1/2}$.